FACHGEBIET HYDROMECHANIK - TECHNISCHE UNIVERSITÄT MÜNCHEN

M.Sc. in Computational Mechanics

MASTER'S THESIS

Modeling Drag Reduction in Turbulent Flows by Brownian Fiber Additives

ISMAIL DUYAR

Supervisor : **Dr.-Ing. Amin Moosaie**

Examiner : **Univ.-Prof. Dr.-Ing. habil. Michael Manhart**

Munich, December, 2011

Ethics Declaration

I hereby declare that this thesis submitted for the Master of Science degree to the Fachgebiet Hydromechanik at the Technische Universität München is my own work. All the informations in this document have been obtained and presented in accordance with academic rules and ethical conduct. I also declare that, as required by these rules and conduct, I have fully cited and referenced all material and results that are not original to this work.

München, 09.12.2011

Ismail Duyar

Abstract

A new algebraic closure model for the non-Newtonian Navier-Stokes equations has been proposed in order to get more realistic turbulent statistics for dilute Brownian fiber suspensions in wall-bounded turbulent flows. Our new model is an improvement on existing VAF model which is capable of showing the basic features of drag reducing behavior of the non-Brownian fibers. Our new model (VAFB) also considers the Brownian motion of the fiber additives. Two-way coupled simulations of fully-developed turbulent channel flows have been conducted with a nominal shear Reynolds number of $\mathrm{Re}_\tau = 180$ with different rotary Brownian diffusivities in order to show the effects of the Brownian motion in turbulent flows. A validation has been done by comparing the results with those of VAF model with the same flow configuration. After simulating different test cases with different Péclet numbers, we have presented the mean streamwise velocity, the turbulence intensity, the Reynolds shear stress and the mean non-Newtonian stress profiles. Results have shown that when the intensity of the Brownian motion increases, the flow tends to the Newtonian state. Therefore, we get the maximum drag reduction in case of high Péclet numbers. We also observed that when the Péclet number is 100, the results of that specific flow case are very similar to those of the Newtonian flow, and by further increase in Brownian diffusivity produces not a drag reduction but a frictional drag increase in the flow. These findings are in accordance with the previous findings in literature. Therefore, VAFB model is able to represent the main characteristics of wall-bounded turbulent flows of dilute Brownian fiber suspensions with a significant decrease in computational costs when compared to that of direct solution of Fokker-Planck equation.

“Science is the most reliable guide for civilization, for life, for success in the world. Searching a guide other than the science is carelessness, ignorance and heresy.”

Mustafa Kemal ATATÜRK

Acknowledgments

First of all, I would like to thank my examiner Univ.-Prof. Dr.-Ing. habil. Michael Manhart for his guidance and giving me a chance to work in this specific topic. I also want to thank my adviser Dr.-Ing. Amin Moosaie for his priceless supervision throughout my thesis.

This master thesis is supported and funded by “BOTAS Petroleum Pipeline Corporation” which is the main natural gas and crude oil supplier in Turkey. I would like to express my gratitude to my company administrators for not only supporting me during my master education, but also giving me the opportunity to work in such an important topic.

Especially, I would like to thank my father, my mother and my girlfriend Serap for their patient love throughout my life. Without their everlasting love and support, I would not be able to finish my master thesis.

This work is dedicated to Mustafa Kemal ATATÜRK who is a very important person for me and one of the most memorable supporters of science and technology across the globe.

Table of Contents

List of Figures

List of Tables

1 INTRODUCTION

1.1 Background

It is discovered by scientists that adding a little amount of additives such as long-chained polymers, fibers (rigid rod-like polymers), etc. into wall-bounded turbulent flows reduces the drag caused by friction in the flow. The frictional drag reduction is in significant levels. It is found that the frictional drag can be reduced by up to 80% by adding polymers and by up to 26% by adding fibers into the pipe flow. The amount of polymers, fibers and the other additives which are added to the flow are considerably low. Only few parts per million (ppm) of additives with respect to the suspension itself could exhibit drag reduction. During the last decades the researches on this subject increased considerably across the globe. However, due to the complicated structure of turbulence and lack of knowledge of the additives' effects on turbulent flows, there are still too many things left undiscovered for this problem. Therefore, this subject needs to be studied and the simulation techniques should be improved not only because of its industrial importance, but also due to its significance for scientists to understand the main mechanisms behind the drag reduction.

Drag reducing behavior of the additives has been known for more than sixty years. The first discovery of that specific topic has been made by Toms in 1948, since when this drag reducing behavior of the additives has been known as the Toms phenomenon. He discovered that a polymeric solution exhibits less drag when compared to the solvent in a pipe. After that time many scientists have focused on that specific topic and made many theoretical and experimental studies in order to understand the basics of drag reduction in wall bounded turbulent flows. Their studies and experiments have shown that, after adding these additives into the flow, the intensity of turbulence has been decreased by means of an unknown mechanism. Therefore, it is important to understand the main mechanism behind this drag reduction. Until the last decades, only experimental and theoretical studies have been done due to the lack of computational power to simulate a turbulent flow which is one of the most important engineering problems in today's science and technology, and requires more knowledge for a full enlightenment. However, in the

past two decades direct numerical simulation (DNS) techniques become possible for the simulation of turbulent flows. In direct numerical simulations, Navier-Stokes equations are solved without any turbulence model such as LES, DES, RANS etc. In DNS these equations are solved on a fine grid by using small time steps. So, even the smallest scales of turbulent flows can be captured. However, in order to resolve all scales of the turbulence, it is important to use simple constitutive models, and it is necessary to work with low Reynolds numbers. Since, it is proved by scientists that the computational costs increase with Re^3. Therefore, it is not just a need but a must to work with low Reynolds numbers. Now, let me make a summary about the researches in our topic and mention the experimental and theoretical findings which I will be dealing with throughout this master thesis. According to Gennes [5], the drag reduction is obtained by the elastic effects of the additives. This theory has also been supported by Sreenivasan and White [21]. According to above mentioned researchers the main mechanism behind this drag reduction was elasticity. So, they were supporting the idea that such a drag reduction may be possible in the presence of flexible polymers. However, Sasaki [20] discovered that dilute solutions of Xanthan gum also exhibit such drag reduction. Here, Xanthan gum can be considered as a rigid rod-like particle. Lee et *al.* [11] used a mixture of polymer and fiber (rigid rod-like polymers) additives, and they observed that these mixtures not only increase the drag reducing property significantly, but also exhibit more shear resistance. By using a mixture of fibrous and polymeric additives, they also surpassed the so-called maximum drag reduction (MDR) asymptote of Virk et *al.* [23]. Therefore, it is deduced that elasticity is not the only mechanism behind the drag reduction. Lumley [12] was the first researcher who has suggested that there is a strong relation between the increase of extensional viscosity and the decrease in the amount of the near-wall turbulent structures. Also, Landahl [10] conclude his theoretical studies on this subject with an idea such that, the anisotropy caused by the extended rigid particles is one of the key properties and has significant effects on drag reduction. This theory has also been supported by Hinch [8] and Metzner [15]. They have suggested that fibers and polymers exhibit different mechanisms while they are reducing the drag. According to their studies, in case of rigid rod-like particles, extensional viscosity was the main mechanism behind this drag reduction. Later, these theories have been supported by the results of den Toonder *et al.* [22], Manhart and Friedrich [13] and Moosaie and Manhart [17].

Den Toonder *et al.* [22] neglected the effects of elasticity and considered a model containing rigid-rod like polymers or fibers. They conducted a direct numerical simulation

for a turbulent pipe flow in order to investigate the effects of the fibers. Because of the high computational costs of direct numerical simulations, they came up with the idea that the fibers are parallel to the local flow velocity vector. It means that the fibers are fully aligned with the direction of the local velocity vector. In spite of this simplifying assumption his model was able to capture the basics of the drag reduction and the main turbulence statistics which are parallel with the experimental findings. They called his model as the viscous anisotropic (VA) model. Later, Manhart and Friedrich [13] have used the VA model for a turbulent channel flow. They found that by means of this simplified model, drag reduction can also be obtained in turbulent channel flows. Lately, in order to obtain more realistic turbulent statistics Moosaie and Manhart [17] has improved the viscous anisotropic model of den Toonder *et al.* [22] to alter some undesirable effects of the VA model. This improved model is based on the assumption that fibers are aligned with the local velocity fluctuation vector. They called this new model as the VAF model. The results have shown that the unwanted characteristic of the VA model have been altered by the VAF model.

In this master thesis, our purpose is to improve the VAF model of Moosaie and Manhart [17] by taking the Brownian motion of the fibers into account. To do so, a new proposal for the calculation of second moment of the Orientation distribution function (ODF) is offered by including the rotary Brownian diffusivity. Two-way coupled simulations have been performed in order to check our new model. The simulations have been conducted in a fully-developed turbulent channel flow with different Péclet numbers. The results have shown that, the new model is also able to exhibit the main characteristics of the drag reducing properties of the dilute suspensions of the Brownian fibers in a Newtonian solvent.

The rest of the thesis will be organized as follows. In this chapter, we will continue on giving background informations. To do so, a detailed explanation of the drag will be given. Also, we will distinguish between the laminar and the turbulent boundary layers, and try to explain the basic mechanism behind the frictional drag with the help of these boundary layers. We will conclude the first chapter with the importance of drag reduction and talk about some industrial applications in this field and emphasize why companies should use these methods in a financial framework. In the second chapter we will try to explain the theoretical background containing the governing equations of the fluid consisting of a Newtonian fluid and fibers. While getting closer to our final governing equations, one will notice all relevant equations which are important to understand the final state of the

governing equations. Also, existing algebraic closure models such as the viscous anisotropic (VA) and the VA model with velocity fluctuations (VAF) will be explained in detail. In chapter 3, we will make our new proposal for Brownian fibers. This new model is called the VAFB model. The basic features of the VAFB model and its theory will be explained in detail. Chapter 4 explains the numerical methods that have been used in our simulations. Also, simulation parameters and all relevant data will be explained in this specific chapter. We will present our results in chapter 5. Finally, we will conclude this master thesis with chapter 6.

1.1.1 What is Drag ? (A Physical Background)

One may simply define drag as a resistance force which tries to decrease the velocity of the moving object. Note that the moving object might be a solid or a fluid. There are several types of drag. Form Drag or Pressure drag occurs due to the form or the shape of the object. Size and shape of the object are the most important parameters for understanding the behavior of the form drag. In general, large bodies with higher cross-sections are subjected to a higher value of form drag force. For example, if we consider an airplane, it can be understood that streamlining the body and the wings will decrease the form drag force. In figure 1.1 one can see the effect of the shape of the object on a fluid flow around a body. In first figure, there is a sphere which has a circular cross-section, and in the other figure there is a streamlined object. One can obviously say that there will be less drag which tries to decrease the moving object's velocity in figure 1.1.b because of its shape. Form drag can be calculated by the drag equation:

$$F_D = \frac{1}{2}\rho\, V^2 C_D A, \tag{1.1}$$

where F_D, ρ, V, C_D and A are the drag force, the density of the fluid, the velocity of the moving object, the drag coefficient and the cross-sectional area of the moving body respectively. One can understand from the above equation that form drag will increase with the square of the velocity. So, if the velocity is doubled, the drag force will be four times the initial value of the drag force. Therefore, especially in high speed vehicles, engineers try to tolerate this disadvantage by streamlining the bodies. One of the other types of drag is the wave drag which is a phenomenon for aircrafts arises at supersonic speeds. However, in this master thesis it will not be explained in detail. Another, and for our thesis the most important type of drag is the frictional drag. In this master thesis, understanding the main mechanisms behind the frictional drag reduction in wall bounded

turbulent flows will be one of our basic goals. That is why, the properties of this specific type of drag and the mechanisms behind it will be discussed in detail. Frictional drag is caused by the interaction of the fluid and the body. If the total area of the object having contact with the fluid is increased, frictional drag will be increased as well. Let us consider figure 1.1 again. One can see that, in figure 1.1.b the total area of the solid object having contact with the fluid is much larger than figure 1.1.a. Therefore, the frictional drag in the figure1.1.b will be much higher than the frictional drag in figure1.1.a. It is also possible to calculate the frictional drag force. To do so, let us consider a pipe or a channel flow with a Newtonian fluid such as water. According to the Newton's law of viscosity, every moving layer moves with different velocities. The layer having contact with the surface has zero velocity. This is called zero slip or no slip condition. It is also said that this layer wets the surface. Although this layer has zero velocity, at some distance from the surface, the velocity should be equal with the velocity of the outer fluid U_∞.

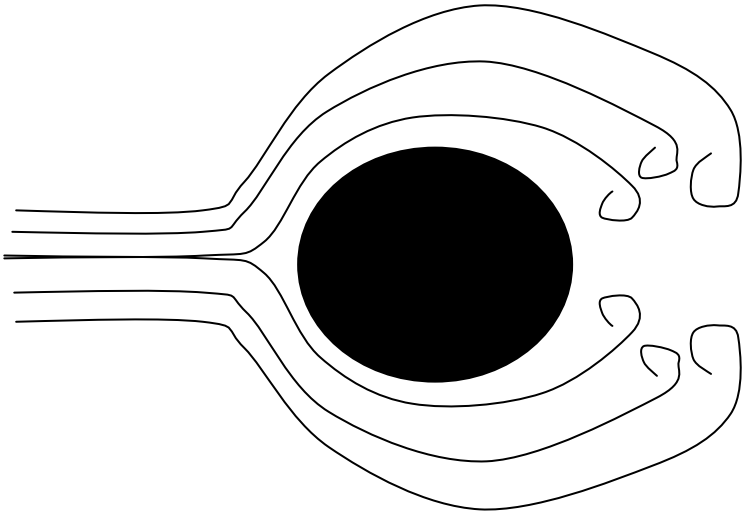

a) Flow around a circular object (sphere)

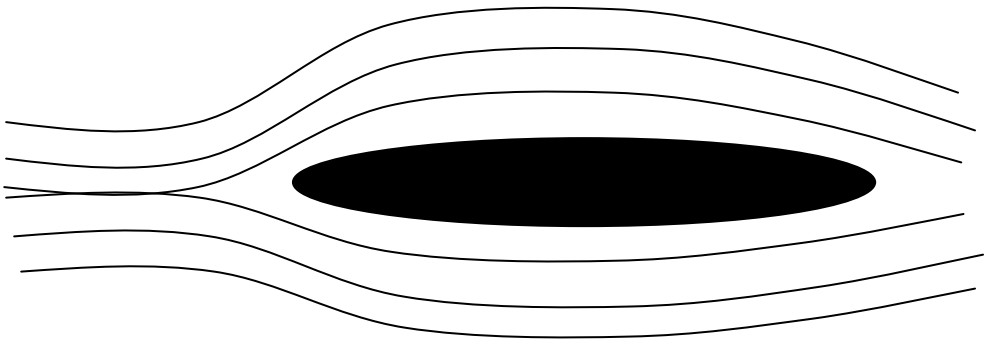

b) Flow around a more streamlined object

Figure 1.1 : Effect of the shape of an object on fluid flow around a body

The region from the surface to that specific height is called boundary layer. Boundary layer is a very thin region compared to the real domain. However, inside the boundary layer the velocity gradients are in considerable levels such that even though the viscosity of the fluid is very low, viscous stresses may achieve significant levels because of these high velocity gradients. With the help of the viscosity of the fluid, zero velocity layer transfers the momentum to the layer right above it. Therefore, the other layers above the surface have a velocity. So, there is a shearing happening between the layers of the moving fluid. The shear stress between the wetted surface and the first moving layer of the fluid is called wall shear stress and denoted with τ_w. As it can be seen in figure 1.2, the velocity of the moving layers inside the boundary layer increases with the distance from the surface. Now, let me mention the Newton's law of viscosity again. According to the Newton's law of viscosity, the wall shear stress can be written as

$$\tau_w = \mu \frac{\partial u}{\partial y}\bigg|_{y=0}, \tag{1.2}$$

where

τ_w is the wall shear stress,

μ is the dynamic viscosity of the fluid

u is the tangential velocity component

y is the height above the surface

$\frac{\partial u}{\partial y}$ is the velocity gradient normal to the surface.

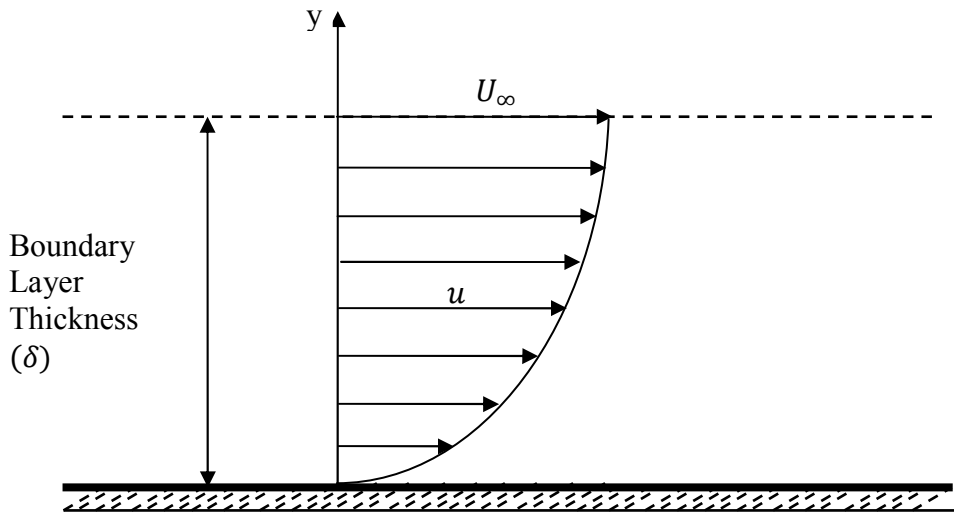

Figure 1.2: Velocity profile inside the boundary layer

Note that according to the formula above, shear stress at a specific height y can also be found. After finding the wall shear stress with equation ((**1**.**2**), one can integrate this stress over the wetted area in order to find the frictional drag force which can be written as

$$F_D = \iint_{\partial\Omega_w} \tau_w \, dA, \tag{1.3}$$

in which $\partial\Omega_w$ is the wall bounded part of the boundary and dA is the integral constant. In a simple form, frictional drag force can be defined as

$$F_D = \tau_w * \ Wetted \ Area. \tag{1.4}$$

In equation ((**1**.**4**) one should notice that wetted area is the area of the object having contact with the fluid. Therefore, if the total area having contact with the fluid increases, the frictional drag will be increased as well. Also, in case of high velocity gradients, wall shear stress τ_w will become higher, so the frictional drag.

1.1.2 Types of the Boundary Layers and the Origin of Turbulent Drag

According to the Newton's law of viscosity, due to the high velocity gradients inside the boundary layer, there will be a stress increase on the surface of the body. The amount of the stress increase depends on the flow type. Now, we will consider different types of boundary layers. There are two types of boundary layers such as laminar boundary layer and turbulent boundary layer. One can compare these boundary layers with the help of figure 1.3. Obviously, it can be seen in figure 1.3.a that, in a laminar boundary layer the flow is steady and smooth. As a result, the boundary layer is very thin. The velocity gradient at the surface, causing a skin friction, is in considerable levels and cannot be neglected; however, it is very small in laminar boundary layers. Now, let us take a look at the turbulent boundary layer. In turbulent boundary layers, flow is neither steady nor smooth as compared to the laminar boundary layers. In addition, we can see eddies arise in turbulent boundary layers. Since the flow is not smooth and contains eddies, the boundary layer is still thin but much thicker than its laminar counterpart. Also, because of the eddying structure, there is and energy exchange between the inner and outer layers in considerable levels. This momentum exchange is one of the most significant key issues for understanding the mechanism of the frictional drag. Because of that situation, the near-wall velocities increase dramatically in turbulent boundary layers. Of course, velocity gradients will be increased as well. That is why, the frictional drag in turbulent boundary layers is much higher than the frictional drag in laminar boundary layers.

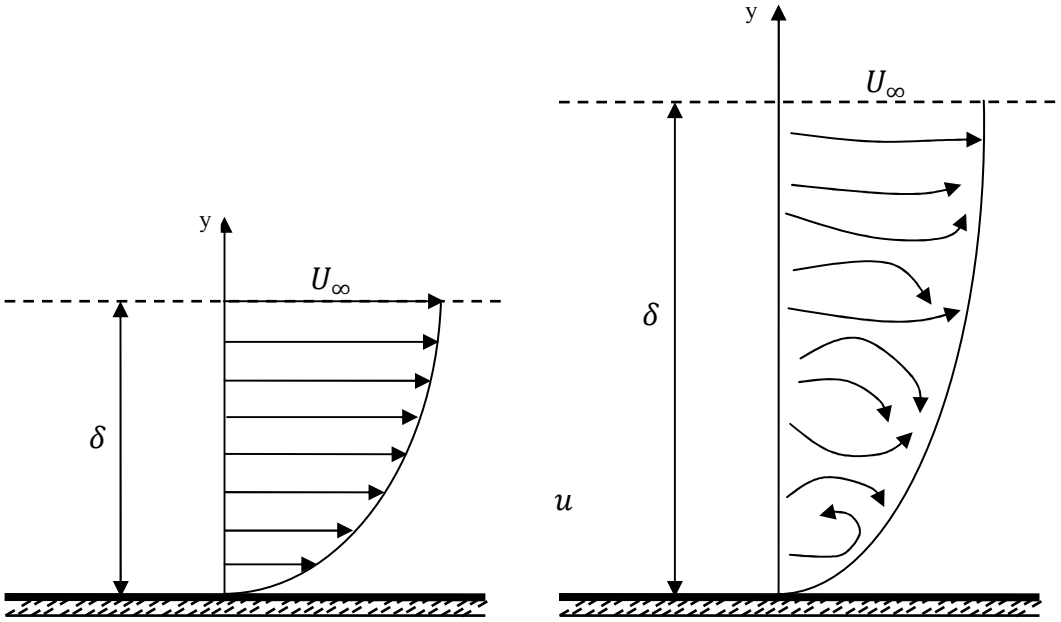

a) Laminar Boundary Layer b) Turbulent Boundary Layer

Figure 1.3 : Comparison of laminar and turbulent boundary layers, the first figure belongs to a laminar boundary layer, the second one shows a turbulent boundary layer. In the Turbulent boundary layer, formation of the eddies can be seen clearly. These eddying structures are the most important reasons causing a higher value of drag force.

Therefore, one can obtain a drag reduction by destroying these eddies to minimize the energy exchanges and so the velocity gradients near the wall. There are different types of methods for eliminating these near-wall coherent structures. In addition to additives such as polymers, fibers, surfactants etc., there are also active control techniques. In this master thesis we will focus on rigid-rod like polymer additives or fibers.

1.1.3 Importance of Drag Reduction

It is a well known fact that, in today's world; energy is one of the most important fundamentals for People's lives. People need energy sources for transportation, manufacturing necessary items, and transmitting energy services i.e. petroleum, natural gas, etc. We need energy in every part of the day in order to carry on our lives properly. So, it is important for scientists to develop new reliable energy sources which are renewable. Also, finding new technologies to increase the efficiency of our energy sources is another important subject for scientists and attracts attention. Efficiency itself may be a simple word; however, studies on this subject could result in not only a decrease in air pollution, but also saving large amounts of money spent by companies and

governments every year. Now, I will make a short summary about these industrial applications in which drag reducing property of the additives are used.

1.1.4 Industrial Applications of Drag Reduction by Additives

The first industrial application of using the polymer additives as a drag reducer was seen in Trans-Alaska Pipeline System in 1979. Brostow [3] has also suggested using drag reducing property of additives, in fire hoses in order to increase the flow rate. However, the most important commercial usage of drag reducing additives is still injecting them into crude oil in a pipeline to reduce the frictional drag. In Trans-Alaska Pipeline System, the engineers aimed to reduce the energy loss due to the turbulent structures in flow by injecting long chain hydrocarbon polymers into the oil. According to their reports [24], they have started the first tests on 1 April, 1979 in the pump station 1 (PS 1). After getting the first preliminary results positively, drag reducing additives has been initiated in PS 1 on July 1, 1979. In the following years, they have initiated drag reducing additives in several pump stations. It was found that adding a small amount of polymeric additives in crude oil increase the pumping efficiency considerably. There is one simple definition of the term “pumping efficiency” for a company. That is “Money”. It can be thought in a way that while transporting the crude oil via pipelines with the same pump pressure, the amount of oil transported to the next pump station increases after the injection of drag reducing additives. Shortly, the flow rate is increased in the presence of additives. It means that, while consuming exactly the same energy, the amount of transported crude oil will be much higher than that of the original state. Commercially speaking, this property of the additives will make companies save large amounts of money spent for energy resources. Note that in Trans-Alaska Pipeline System, according to their reports, throughput has been increased from 1.44 barrels crude oil per day to 2.13 million barrels per day with drag reduction. So, one can imagine how important it is to use drag reducing additives for a pipeline company. In this master thesis we will be trying to understand the properties of drag reduction by fiber additives in turbulent flows. Also, further improvements in this specific subject will be one of our basic goals in order to obtain more realistic description of the mechanism behind this drag reduction. In addition to that, the basic theories will be explained in detail so as to help young researchers who will be studying in that specific topic in the following years.

2 THEORETICAL BACKGROUND

In this chapter, we will present the governing equations for dilute fiber suspensions. We will start from the simple flow cases and develop our equations step by step in order to understand the impression of the viscous effects in a flow clearly. First, the flow will be assumed as an inviscid flow in which the effects of viscosity are neglected. Under this specific assumption the governing equations will be given. Then the viscous effects will be added to the governing equations. Next, the effects of the additives in the governing equations will be discussed in detail. After obtaining the final governing equations, we will focus on some strategies in order to find the non-Newtonian stress tensor $\boldsymbol{\tau}^{NN}$. To do so, existing algebraic closure models (the VA and VAF models) will be explained.

2.1 Basic Equations

2.1.1 Euler Equations

Euler equations are the governing equations of inviscid flows where the fluid is assumed to be an ideal fluid which has zero viscosity. In a 3D flow we can simply write the conservation of mass (continuity equation) as

$$\frac{\partial \rho}{\partial t} + \frac{\partial (\rho u)}{\partial x} + \frac{\partial (\rho v)}{\partial y} + \frac{\partial (\rho w)}{\partial z} = 0, \tag{2.1}$$

where ρ, u, v and w are the density of the fluid and the velocity components of the fluid in x, y and z directions, respectively. The above equation represents a compressible flow in which the density of the fluid changes with time. In this master thesis we are not dealing with compressible flows. Mainly, we will investigate the behavior of the dilute fiber suspensions in which the assumption of incompressibility can be done without concern. In an incompressible flow the density of the fluid does not change with time so the first term of the above equation will vanish. By the help of some basic algebra and using the Nabla operator, conservation of mass can be simply written as

$$\nabla \cdot \boldsymbol{u} = 0, \tag{2.2}$$

where $\boldsymbol{u}$ is the local velocity vector consists of 3 components u, v and w. The local velocity vector can be shown as follows:

$$\boldsymbol{u} = u\boldsymbol{e_x} + v\boldsymbol{e_y} + w\boldsymbol{e_z},$$

in which $\boldsymbol{e_x}, \boldsymbol{e_y}$ and $\boldsymbol{e_z}$ are the unit vectors in x, y and z directions, respectively. Nabla operator reads

$$\nabla = \frac{\partial}{\partial x}\boldsymbol{e_x} + \frac{\partial}{\partial y}\boldsymbol{e_y} + \frac{\partial}{\partial z}\boldsymbol{e_z}\,.$$

Now, let us have a look at the equation regarding the conservation of momentum for incompressible flows. It can be written as

$$\rho\left(\frac{\partial}{\partial t} + \boldsymbol{u}\cdot\nabla\right)\boldsymbol{u} + \nabla p = 0, \tag{2.3}$$

where p is the pressure and ∇p is so-called the pressure gradient. This equation can be simplified by using the "Material Derivative":

$$\rho\frac{D\boldsymbol{u}}{Dt} = -\nabla p, \tag{2.4}$$

in which

$$\frac{D}{Dt} = \frac{\partial}{\partial t} + \boldsymbol{u}\cdot\nabla.$$

Material derivative defines a change of a quantity with time while moving with a velocity field in a path. It is commonly used in fluid mechanics. Until now, we have written the conversation of mass and momentum for inviscid incompressible fluids in the equations ((**2**.**2**) and ((**2**.**4**), respectively. As it is said at the beginning of this section, Euler equations neglect the effects of viscosity. However, in this master thesis we are dealing with the drag which is a result of viscous properties of the fluids. That is why, the viscous effects cannot be neglected and should be taken into account. Therefore, we cannot make the assumption of inviscid flow anymore. Above equations should be improved by adding the effects of the viscosity of the fluid in the flow.

2.1.2 Navier-Stokes Equations

In Navier-Stokes equations, the missing parameter (viscosity) is taken into account. By improving the equations explained in the previous section, one could obtain the governing equations for an incompressible Newtonian fluid. Conservation of mass has already been written in the previous section. Since there is no effect of viscosity of the fluid in mass conservation, the continuity equation remains unchanged. It reads $\nabla \cdot \boldsymbol{u} = 0$. However, the equation regarding the conservation of momentum is different. There will be a term added into the right hand side of equation ((**2**.**4**) as a result of the viscosity of the fluid. This term is a part of the total stress tensor. So, the conservation of momentum for an incompressible Newtonian fluid can be written as follows:

$$\rho \frac{D\boldsymbol{u}}{Dt} = -\nabla p + \nabla \cdot \boldsymbol{\tau}^{N}, \tag{2.5}$$

in which $\boldsymbol{\tau}^{N}$ is the part of stress tensor assigned by the Newtonian fluid. Now, if we compare equations ((**2**.**4**) and ((**2**.**5**), we can clearly see that the effects of the viscosity of the fluid are added to the system. However, this improvement is also not enough for us. Since, in this work, we are dealing with the non-Newtonian fluids which are, for example, dilute suspensions of rigid fiber additives. That is why, equation ((**2**.**5**) also has to be improved by adding the viscous effects of the fibers. This improvement will be discussed in the following section.

2.1.3 Non-Newtonian Navier Stokes Equation

As it is already mentioned in the previous sections, in this master thesis, one of the most important goals will be to understand the different properties of turbulent flows by adding fibers in to the flow. Let us consider a dilute suspension of fibers in a Newtonian solvent such as water. Although water is a Newtonian fluid, the complete suspension will also exhibit non-Newtonian behaviors due to the added fibers. Therefore, we should improve equation ((**2**.**5**) by adding the non-Newtonian effects caused by the fiber additives. One can simply add the non-Newtonian effects into the Navier-Stokes equations as follows:

$$\rho \frac{D\boldsymbol{u}}{Dt} = -\nabla p + \nabla \cdot \ (\boldsymbol{\tau}^{N} + \boldsymbol{\tau}^{NN}), \tag{2.6}$$

where $\boldsymbol{\tau}^{NN}$ is the contribution of non-Newtonian effects on the stress tensor. We can also say contribution of fiber additives on the stress tensor or simply non-Newtonian stress tensor. Continuity equation is still the same as we described earlier and it reads, $\nabla \cdot \boldsymbol{u} = 0$.

We have just obtained the governing equations for an incompressible dilute suspension consists of a Newtonian solvent and a little amount of additives. The expressions “little amount” or “minute amount” are usually used for describing the amount of the additives added into the flow. Generally, this amount is described by ppm (parts per million) notation. This notation is commonly used in chemistry to describe dilute solutions. It shows the mass fraction between the added fibers and the suspension itself. For example, let us consider a dilute fiber suspension in a turbulent channel flow with a fiber concentration of 10 ppm. It means that for 1 million grams (1 ton) of sample suspension, the weight of the suspended fibers is only 10 grams. This is really a small amount when compared to the fluid itself. The interesting thing is that one can obtain drag reduction with such a small amount of additives.

As a summary, in this section, we have obtained the governing equations of non-Newtonian fluids consisting of a Newtonian fluid and fiber additives. These governing equations are the continuity equation (conservation of mass), and the conservation of momentum, which are described in equations ((**2**.**2**) and ((**2**.**6**), respectively. Now, we will investigate these specific equations in detail. Equation ((**2**.**2**) is a straightforward equation. However, equation ((**2**.**6**) is not easy to handle. Describing the Newtonian part of the stress tensor ($\boldsymbol{\tau}^N$) can be done with a well-known constitutive equation

$$\boldsymbol{\tau}^N = 2\mu\boldsymbol{D}, \tag{2.7}$$

in which μ is the dynamic viscosity of the fluid with the unit [Pa.s]. $\boldsymbol{D}$ is the strain rate tensor [1/s], and can be calculated as

$$\boldsymbol{D} = \frac{(\nabla\boldsymbol{u} + (\nabla\boldsymbol{u})^T)}{2}, \tag{2.8}$$

where $(\nabla\boldsymbol{u})^T$ is the transpose of the velocity gradient tensor. Note that strain rate tensor $\boldsymbol{D}$ is a symmetric tensor. The components of the stain rate tensor can be derived with the following expression:

$$D_{ij} = \frac{1}{2}\left(\frac{\partial u_i}{\partial x_j} + \frac{\partial u_j}{\partial x_i}\right).$$

As a general knowledge, it should be mentioned that, every tensor $\boldsymbol{A}$ can be written as a sum of a symmetric tensor and a skew symmetric (antisymmetric) tensor. This property of the tensors is commonly used in fluid mechanics. In fluid mechanics, we separate the velocity gradient tensor into two parts. First one is the strain rate tensor $\boldsymbol{D}$, and it is a

symmetric tensor which we have already mentioned. The second one is the rotation rate tensor $\boldsymbol{\Omega}$. Rotation rate tensor is a skew symmetric tensor in which the following expression holds; ($\boldsymbol{\Omega} = -\boldsymbol{\Omega}^{\boldsymbol{T}}$). It is also possible to relate the rotation rate tensor to the velocity gradient tensor. This relation reads

$$\boldsymbol{\Omega} = \frac{(\nabla \boldsymbol{u} - (\nabla \boldsymbol{u})^T)}{2}. \tag{2.9}$$

The components of the rotation rate tensor can be written as

$$\Omega_{ij} = \frac{1}{2}\left(\frac{\partial u_i}{\partial x_j} - \frac{\partial u_j}{\partial x_i}\right).$$

If we look at equations ((**2**.**8**) and ((**2**.**9**) carefully, we can see that the sum of the rotation rate and the strain rate tensors gives the velocity gradient tensor. So the following expression holds.

$$\nabla \boldsymbol{u} = \boldsymbol{D} + \boldsymbol{\Omega}. \tag{2.10}$$

Note that there are different notations for these tensors in literature, but of course their meaning is important and this meaning never changes. We will be talking about these tensors more often in the following pages. By means of the above equations, we now have a basic idea of calculating the Newtonian part of the stress tensor. However, how can we define the non-Newtonian part of the stress tensor $\boldsymbol{\tau}^{NN}$? In order to do so, a differential equation (a non-Newtonian constitutive equation) should be obtained. This will be the topic of the following section.

2.2 Non-Newtonian Stress Tensor

In order to obtain a constitutive equation for the non-Newtonian part of the stress tensor, Brenner (1974) has developed a model for dilute suspensions. According to his theory, the additional stress caused by a single axisymmetric rigid particle can be written as

$$\begin{aligned}\boldsymbol{\tau}^{Single} = {} & 2\mu_0 \boldsymbol{D} + \mu_1 \boldsymbol{I}\boldsymbol{D}\boldsymbol{:}\boldsymbol{nn} \\ & + \mu_2(\boldsymbol{D}\boldsymbol{:}\boldsymbol{nnnn}) + 2\mu_3[\boldsymbol{n}(\boldsymbol{D}\cdot\boldsymbol{n}) + (\boldsymbol{D}\cdot\boldsymbol{n}).\boldsymbol{n}] \\ & + 2\mu_4 D_r(3(\boldsymbol{nn}) - \boldsymbol{I}),\end{aligned} \tag{2.11}$$

where $\boldsymbol{\tau}^{Single}$ is the stress due to a single rigid particle. $\boldsymbol{D}$ is the strain rate tensor. $\boldsymbol{n}$ is a unit vector showing the orientation of each particle. $\boldsymbol{I}$ is the identity tensor. D_r is the rotary Brownian diffusivity. μ_0, μ_1, μ_2, μ_3 and μ_4 are the material constants depending on the aspect ratio (r), and volume fraction (ϕ) of the suspended particles and the viscosity of the solvent (μ). These constants depend on known variables and can be calculated easily. Calculation and derivation of these variables for different kind of particles can be found in literature and will not be discussed in this work in detail. One may refer to Brenner [2], and Moosaie [16] in order to get more knowledge about the derivation these material constants. In equation ((**2**.**11**) only one single particle is considered; however, if we think about a suspension of rigid fibers, there are large quantities of fibers which are oriented in a random manner. Therefore, in order to obtain the non-Newtonian part of the stress tensor $\boldsymbol{\tau}^{NN}$, one could do an averaging. So, $\boldsymbol{\tau}^{NN}$ can be obtained by a little modification on equation ((**2**.**11**):

$$\begin{aligned}\boldsymbol{\tau}^{NN} = {} & 2\mu_0\boldsymbol{D} + \mu_1\boldsymbol{I}\boldsymbol{D}:\langle\boldsymbol{nn}\rangle \\ & +\mu_2\boldsymbol{D}:\langle\boldsymbol{nnnn}\rangle + 2\mu_3(\langle\boldsymbol{nn}\rangle\cdot\boldsymbol{D} + \boldsymbol{D}\cdot\langle\boldsymbol{nn}\rangle) \\ & +2\mu_4 D_r(3\langle\boldsymbol{nn}\rangle - \boldsymbol{I}),\end{aligned} \tag{2.12}$$

in which $\langle\boldsymbol{nn}\rangle$ and $\langle\boldsymbol{nnnn}\rangle$ are the second and the fourth moments of the orientation distribution function (ODF), respectively. As one can understand from equation ((**2**.**12**) that, calculating the stress caused by the suspended fibers requires knowledge of the orientations of the fibers because $\boldsymbol{\tau}^{NN}$ depends on the second and the fourth moments of the orientation distribution function (ODF) of the fiber additives. The configuration of an axisymmetric rigid rod-like particle can be seen in figure 2.1. In this figure we can see the unit vector $\boldsymbol{n}$ showing the orientation of the particle.

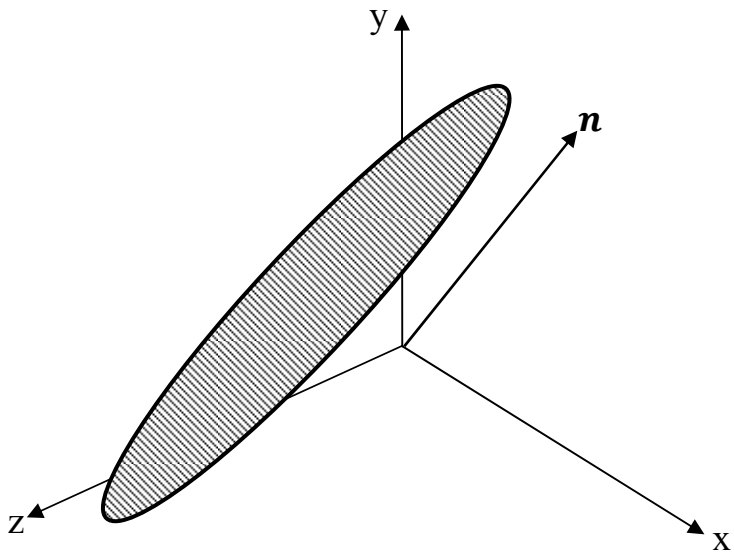

Figure 2.1 : Configuration of an axisymmetric rigid rod-like particle

In order to compute the second and the fourth moments of the orientation distribution function, first we should obtain the orientation vector $\boldsymbol{n}$ for one single particle. Evolution of the orientation vectors has been done by the Jeffery (1922) for ellipsoidal particles inside a viscous fluid. Jeffery's equation can be written as follows:

$$\frac{D\boldsymbol{n}}{Dt} = \boldsymbol{\Omega}\cdot\boldsymbol{n} + \kappa[\boldsymbol{D}\cdot\boldsymbol{n} - (\boldsymbol{n}\cdot\boldsymbol{D}\cdot\boldsymbol{n})\boldsymbol{n}], \tag{2.13}$$

where κ is the shape factor which can be calculated as

$$\kappa = \frac{r^2 - 1}{r^2 + 1}, \tag{2.14}$$

in which r is the aspect ratio of the fibers with $r = L/a$. Here, L and a are the half length and the equatorial radius of the fibers respectively. Note that it is also possible to write the last term in equation ((**2**.**13**) $(\boldsymbol{n}\cdot\boldsymbol{D}\cdot\boldsymbol{n})\boldsymbol{n}$ as $\boldsymbol{D}:\boldsymbol{nnn}$. If we take a look at the definition of the shape factor κ, one can clearly see that, if the aspect ratio r goes to 1; κ will be 0. It shows the case that the particles are sphere. In case of spherical particles one could not talk about an anisotropic behavior of the suspension. We can discuss this condition by the help of equation ((**2**.**13**). In case of spherical particles the last term of equation ((**2**.**13**) will vanish. It means that the particles will be orientated by means of the rotation rate tensor **Ω**. Note that in case of rigid rod-like particles the value of κ will be equal to 1. So, in case of rigid fibers equation ((**2**.**13**) reduces to

$$\frac{D\boldsymbol{n}}{Dt} = \boldsymbol{\Omega} \cdot \boldsymbol{n} + \boldsymbol{D} \cdot \boldsymbol{n} - \boldsymbol{D} : \boldsymbol{nnn}. \tag{2.15}$$

In equation ((**2**.**13**), the symbol : denotes a second order tensor contraction. In order to find the second moment of the orientation distribution function, one can follow Advani & Tucker (1987):

$$\begin{aligned}\frac{D\langle \boldsymbol{nn}\rangle}{Dt} &= \boldsymbol{\Omega} \cdot \langle \boldsymbol{nn}\rangle + \langle \boldsymbol{nn}\rangle \cdot \boldsymbol{\Omega}^{\boldsymbol{T}} \\ &+\kappa(\boldsymbol{D} \cdot \langle \boldsymbol{nn}\rangle + \langle \boldsymbol{nn}\rangle \cdot \boldsymbol{D} - 2\boldsymbol{D} : \langle \boldsymbol{nnnn}\rangle) \\ &+2D_r(\mathbf{I} - 3\langle \boldsymbol{nn}\rangle),\end{aligned} \tag{2.16}$$

where D_r is the rotary Brownian diffusivity. If we take a closer look at equation ((**2**.**16**), we can see that for derivation of the second moment of the orientation distribution function, the fourth moment of the ODF should be known. Therefore, the above equation is not algebraically closed. So, one needs a suitable closure model in order to solve the equation ((**2**.**16**). As we have already explained, in order to reproduce the non-Newtonian part of the stress tensor one should find the moments of the ODF. There are different options to do this. The first one is called the moment approximation method in which the equation ((**2**.**16**) is solved with a suitable closure model which will be discussed in this master thesis. The second way is to solve the so-called Fokker-Planck equation directly to obtain the fiber conformation. Fokker-Planck equation reads

$$\frac{D\Psi}{Dt} = \underbrace{-\nabla_{\mathrm{n}} \cdot \left(\Psi \frac{D\boldsymbol{n}}{Dt}\right)}_{\text{Drift Term}} + \underbrace{D_r \Delta_n \Psi}_{\text{Diffusion Term}}, \tag{2.17}$$

where ∇_{n} and Δ_n are the Nabla and Laplace operators defined on the surface of the unit sphere, respectively. $\Psi(\boldsymbol{n}; \boldsymbol{x}, t)$ is the orientation distribution function (ODF) which can be defined as the volume fraction of the particles which are oriented in the direction of $\boldsymbol{n}$ at a given point $\boldsymbol{x}$ at time t. Fokker-Planck equation contains a drift and a diffusion term. Drift term is the first term in right hand side of equation ((**2**.**17**). It stresses the effect of the fluid via rotation rate ($\boldsymbol{\Omega}$) and strain rate ($\boldsymbol{D}$) tensors. Diffusion term is the last term in the right hand side of equation ((**2**.**17**) and stresses the effect of the rotary Brownian motion. In other words, the strain rate tensor, the rotation rate tensor and the rotary

Brownian diffusivity are the key parameters for solving the Fokker-Planck equation and understanding the orientation dynamics of the fibers. Note that the time derivative of the orientation vector $\frac{D\boldsymbol{n}}{Dt}$ which appears in equation ((**2**.**17**) can be calculated by equation ((**2**.**13**). In literature, direct solution techniques of the Fokker-Planck equation are available. After solving the Fokker-Planck equation one can calculate the second and the fourth moments of the orientation distribution function. However, this method is computationally very expensive and will not be discussed in this master thesis. Therefore, we turn back our moment approximation method again. Moment approximation method works with a suitable closure model. There are several methods offered by scientists to close equation ((**2**.**16**) algebraically. Widely used closure models can be classified as linear closure model, quadratic closure model, hybrid closure model, Hinch & Leal closure model and Invariant-Based Optimal Fitting closure model (IBOF). In this master thesis we are going to use the quadratic closure. According to this closure model, the fourth moment of the orientation distribution function is a function of the second moment of the ODF. Quadratic closure model reads

$$\langle \boldsymbol{nnnn} \rangle = \langle \boldsymbol{nn} \rangle \langle \boldsymbol{nn} \rangle. \tag{2.18}$$

In the following sections some algebraic closure models will be presented in order to close the non-Newtonian Navier stokes equations with reasonable computational costs.

2.3 Viscous Anisotropic (VA) Model

In moment approximation approach, in order to solve the non-Newtonian governing equations ((**2**.**2**) and ((**2**.**6**) with ((**2**.**16**) along with a quadratic closure model, one still needs powerful computation resources. Especially, in case of turbulent flows, while capturing even the smallest scales of the turbulence, these computational costs would be in significant levels and that would be a really heavy burden for all researchers. Although, the moment approximation methods are less expensive than the direct solution methods of the Fokker-Planck equation, still we have enough equations to solve and implement. Therefore, den Toonder *et al.* [22] have proposed a model for the suspensions containing large aspect ratio fibers and Newtonian fluids. According to their assumption, the fibers align quickly with the local velocity vector. Mathematically, this further simplification states the following relation for the orientation of a single particle:

$$\boldsymbol{n} = \frac{\boldsymbol{u}}{|\boldsymbol{u}|}, \tag{2.19}$$

in which $\boldsymbol{u}$ is the local velocity vector and $|\boldsymbol{u}|$ is the magnitude of the local velocity vector. Note that in mathematics, every unit vector can be written as a vector divided by its magnitude. Here, $\boldsymbol{n}$ is a unit vector showing the orientation of the particle. By using equation ((**2**.**19**), the second moment of the orientation distribution function reads

$$\langle \boldsymbol{nn} \rangle = \frac{\boldsymbol{uu}}{\boldsymbol{u} \cdot \boldsymbol{u}}. \tag{2.20}$$

By following equation ((**2**.**18**) the fourth moment of the ODF can be written as

$$\langle \boldsymbol{nnnn} \rangle = \frac{\boldsymbol{uuuu}}{(\boldsymbol{u} \cdot \boldsymbol{u})^2}. \tag{2.21}$$

Now, we have everything in hand in order to calculate the non-Newtonian stress tensor $\boldsymbol{\tau}^{NN}$. According to den Toonder *et al.* [22], non-Newtonian stress tensor for high-aspect-ratio non-Brownian fibers can be written as

$$\boldsymbol{\tau}^{NN} = \mu_2 \boldsymbol{D} : \langle \boldsymbol{nnnn} \rangle. \tag{2.22}$$

Recalling den Toonder's aligned-particle approximation, the non-Newtonian Stress tensor reads

$$\boldsymbol{\tau}^{NN} = \mu_2 \boldsymbol{D} : \frac{\boldsymbol{uuuu}}{(\boldsymbol{u} \cdot \boldsymbol{u})^2}, \tag{2.23}$$

where μ_2 is a material constant with the following definition:

$$\mu_2 = \frac{\pi \mu n l^3}{6 \ln(2r)}, \tag{2.24}$$

in which l is the length of the suspended fibers and r is their aspect ratio.

The model described by equation ((**2**.**24**) is called the viscous anisotropic (VA) model. In the VA model, elastic effects are totally neglected, and it shows only viscous effects. By using the VA model, den Toonder *et al.* [22] were able to exhibit the drag reduction in turbulent pipe flows. Later, Manhart and Friedrich [13] also used the VA model in turbulent channel flows. They also observed the drag reduction in turbulent channel flows. Therefore, one can conclude that, the VA model was able exhibit drag reduction in wall-bounded turbulent flows with a small amount of computational cost when compared to the direct solutions of Fokker-Planck equation. Although the VA model is capable of showing

the basic behaviors of drag reduction, there are some defects in this model. For instance, the VA model is a Galilean variant. This means that the non-Newtonian stress tensor defined by equation (2.30) can be changed with a moving reference system. However, we should always obtain the same stress regardless of the reference system. In addition to that the VA model also suffers from predicting the normal non-Newtonian stress component $\langle \tau_{11}^{NN} \rangle$. The VA model calculates this component as a negative value away from the wall; however, by direct solution of the Fokker-Planck equations, its found that the normal non-Newtonian stress does not have negative values away from the wall. One may refer Moosaie and Manhart [17] for a detail information about these unwanted behaviors of the VA model. In spite of its drawbacks, the VA model is still an important model and need to be improved due to the low computational costs it provides. As an improvement to the VA model, Moosaie and Manhart [17] has modified the VA model and proposed another model in order to remove unwanted behaviors of the VA model. This will be the topic of the next section.

2.4 VA Model with Velocity Fluctuations (VAF Model)

In order to improve the VA model, Moosaie and Manhart [17] have proposed another idea. According to their proposal, suspended fibers are aligned with the local velocity fluctuation vector $\boldsymbol{u}'$. With this proposal the unit vector $\boldsymbol{n}$ which gives the orientation of the suspended particles reads

$$\boldsymbol{n} = \frac{\boldsymbol{u}'}{|\boldsymbol{u}'|}, \tag{2.25}$$

in which $\boldsymbol{u}'$ is the local velocity fluctuation vector and $|\boldsymbol{u}'|$ is the magnitude of the local velocity fluctuation vector. Note that in turbulent flows the local velocity vector $\boldsymbol{u}$ can be split into two different quantities. These quantities are the average and the fluctuating parts of the local velocity vector. Therefore, the below expression holds:

$$\boldsymbol{u} = \langle \boldsymbol{u} \rangle + \boldsymbol{u}', \tag{2.26}$$

where $\boldsymbol{u}$, $\langle \boldsymbol{u} \rangle$ and $\boldsymbol{u}'$ are the local velocity vector, the mean velocity vector and the velocity fluctuation vector, respectively. This is called Reynolds decomposition. According to this new proposal, the second and the fourth moments of the ODF can be written as

$$\langle \boldsymbol{nn} \rangle = \frac{\boldsymbol{u'u'}}{\boldsymbol{u'} \cdot \boldsymbol{u'}} \ , \tag{2.27}$$

$$\langle \boldsymbol{nnnn} \rangle = \frac{\boldsymbol{u'u'u'u'}}{(\boldsymbol{u'} \cdot \boldsymbol{u'})^2} \ . \tag{2.28}$$

Note that the term $\boldsymbol{u'} \cdot \boldsymbol{u'}$ is two times the turbulent kinetic energy (TKE) which can be written as the following expression:

$$(TKE) = \frac{1}{2} \left(u'^2 + v'^2 + w'^2 \right). \tag{2.29}$$

According to the VAF model, the non-Newtonian stress tensor can be written as follows:

$$\boldsymbol{\tau}^{NN} = \alpha \mu \boldsymbol{D} : \frac{\boldsymbol{u'u'u'u'}}{(\boldsymbol{u'} \cdot \boldsymbol{u'})^2} \ , \tag{2.30}$$

where α is a model parameter which depends on the concentration of the fibers and their aspect ratio. The model parameter α reads

$$\alpha \ = \frac{\phi r^2}{\ln r} \ , \tag{2.31}$$

in which r is the aspect ratio of the fibers and ϕ is their volume fraction and can be defined as follows:

$$\phi = \frac{4\pi n L^3}{3r^2} , \tag{2.32}$$

where n and L are the number density and the half-length of the fibers respectively. The term nL^3 is also known as the concentration parameter.

The model described by equation ((**2.30**) is called the viscous anisotropic model with velocity fluctuations (VAF model). The VAF model is also able to exhibit the main drag reducing behavior of the dilute fiber suspensions. In contrast to the VA model, the VAF model is Galilean invariant. It is a very important property that cannot be obtained by VA model. In addition to that, the VAF model produced more realistic results in predicting the non-Newtonian stresses. Unlike the VA model, in the VAF model the normal non-Newtonian stress $\langle \tau_{11}^{NN} \rangle$ is not negative away from the wall. This is also another important property of the VAF model that the VA model is unable to satisfy. Both the VA and VAF models are using non-Brownian fibers which are assumed to be unaffected from the Brownian motion in the flow. However, in case of microfibers or tiny particles, Brownian

motion plays an important role for understanding the drag reducing behavior of the fiber additives. In this master thesis, our goal is to propose a new model for Brownian fibers in order to get more realistic turbulent statistics for non-Newtonian fluids containing a Newtonian solvent with rigid fiber additives. Basically, this proposal will be a modification of the VAF model of Moosaie and Manhart [17]. In the following chapter this new proposal will be presented in detail. Also, the basic properties of the Brownian motion and its theoretical background will be given. Additionally, all necessary equations will be modified by taking the Brownian motion of the particles into account.

3 VAF MODEL WITH BROWNIAN MOTION (VAFB MODEL)

In this chapter, a new proposal for the second moment of the orientation distribution function will be presented. This new proposal also considers the effects of the Brownian motion of the fibers. After this part of the thesis, we will call this new model as the VAFB model. The letter "B" implies the Brownian motion. In order to achieve the current state of the VAFB model, we had to make another proposal. It is proved that the first proposal cannot be used as a closure model. In the following pages one will see this eliminated proposal and the reasons why we cannot use it. Then, we have offered our second proposal for the second moment of the ODF. The second proposal (the VAFB model) has successfully exhibited the drag reducing behavior of the Brownian fibers. Before explaining these proposals and their results in detail, I will make a short summary about the theory of the Brownian motion which is one of the most important key issues in this master thesis.

3.1 Brownian Motion

Brownian motion is the random motion of a tiny particle in a fluid. Note that this fluid might be a liquid or a gas. This phenomenon has been discovered by a Botanist Robert Brown while he was making a research with pollen grains. He observed with a microscope that pollen grains are moving randomly on the surface of water. After that time this phenomenon has been known as Brownian motion. The reason why we are dealing with this movement is that, if the fibers are small enough, then they will also be affected by this motion in the fluid. Therefore, understanding the behavior of the Brownian motion is very important for us. For a spherical particle, as Einstein (1905) suggested, the Brownian diffusivity D can be written as

$$D = \frac{k_B\, T}{\gamma}, \tag{3.1}$$

in which D, k_B, T and γ are the Brownian diffusivity, the Boltzmann constant, the absolute temperature and the Stoke's drag coefficient, respectively. For an elongated particle such as a high-aspect-ratio fiber, Brownian motion can be split into two different types which are the spatial and the rotary Brownian motions. Note that in case of spherical particles, rotary Brownian motion is not important; however, this motion is very important in case of fibers. Rotary and spatial Brownian motions can be written as follows:

$$D_r \propto \frac{k_B\, T}{\mu l^3}, \tag{3.2}$$

$$D_s \propto \frac{k_B\, T}{\mu l}, \tag{3.3}$$

where D_r, D_s, μ and l are the rotary Brownian diffusivity, the spatial Brownian diffusivity, the dynamic viscosity of the fluid and the fiber length, respectively. Note that we are considering fibers which have high aspect ratios, but their lenghts are much smaller than 1 ($l \ll 1$). As it can be understood from the above equations, D_r will be much higher than D_s. Therefore, the spatial Brownian diffusivity can be neglected. Brownian motion is characterized by a well-known dimensionless number, so called the Péclet (Pe) number. Rotary Pe number is defined as

$$Pe_r = \frac{\dot{\gamma}}{D_r}, \tag{3.4}$$

where $\dot{\gamma}$ is the shear rate and can be found as; $\dot{\gamma} = u_b * h$, in which u_b and h are the bulk velocity and the channel half width, respectively. In our simulations, the value of bulk velocity is known. We will talk about that in chapter 4 while explaining our flow solver MGLET. The value of the bulk velocity is $u_b = 1m/s$, and the channel half width is $1m$. Therefore, shear rate of the flow is $\dot{\gamma} = 1/s$. So it can be deduced from above equations that the only parameter that might change the Pe number is the rotary Brownian diffusivity and so the length of the fibers. In case of long fibers, the value of D_r will be low. And therefore, Pe number will be bigger, and in that case we can talk about a weak Brownian motion. However, in case of short fibers, the result will be vice versa, Pe number will be a low value. In that case and the motion is a strong Brownian motion.

Before presenting the new proposal to account for the effect of the Brownian motion, we will now explain Hinch and Leal's (1975, 1976) rheological theory. Hinch and Leal's

findings provide an important reduction in equation ((**2**.**12**). One may also refer to Moosaie (2011) for detail information. According to Hinch & Legal's proposal, the non-Newtonian stress tensor $\boldsymbol{\tau}^{NN}$ can be written as follows:

$$\boldsymbol{\tau}^{NN} = 2\mu\phi\,[2A\boldsymbol{D}:\langle\boldsymbol{nnnn}\rangle + 2B\,(\langle\boldsymbol{nn}\rangle\cdot\boldsymbol{D} + \boldsymbol{D}\cdot\langle\boldsymbol{nn}\rangle) + C\boldsymbol{D} + FD_r\langle\boldsymbol{nn}\rangle], \tag{3.5}$$

where ϕ is the volume fraction of the fibers and A, B, C and F are the material constants which depend on the aspect ratio of the fibers r. Their asymptotic forms, for high aspect ratios $r \to \infty$, are also given in their publications as follows.

$$A = \frac{r^2}{4(\ln(2r) - 1.5)}, \tag{3.6}$$

$$B = \frac{3(\ln(2r) - 5.5)}{r^2}, \tag{3.7}$$

$$C = 2, \tag{3.8}$$

$$F = \frac{3r^2}{\ln(2r) - 0.5}, \tag{3.9}$$

It can be deduced from the above equations that for large aspect ratios, the constant B will be zero due to the term r^2 in its denominator. This means that for increasing values of r, B will converge to zero. Also, the constant C is always 2 and can be neglected for high aspect ratio fibers. Therefore, only two coefficients will remain in case of slender fibers (high aspect ratio fibers). So, the equation ((**3**.**5**) reduces to the following:

$$\boldsymbol{\tau}^{NN} = 2\mu\phi\,[2A\boldsymbol{D}:\langle\boldsymbol{nnnn}\rangle + FD_r\langle\boldsymbol{nn}\rangle]. \tag{3.10}$$

According to equation ((**3**.**10**) non-Newtonian part of the stress tensor can be approximated by finding only two material constants A and F. The derivation of these constants can be done as following:

$$A = \frac{r^2}{4(\ln(2r) - 1.5)} = \frac{r^2}{4(\ln 2 + \ln r) - 1.5)} = \frac{r^2}{4\ln 2 + 4\ln r - 6}$$

There is a well known property of logarithm, it reads

$$\log(a * b) = \log a + \log b \quad \text{so; } \ln(2r) = \ln 2 + \ln r.$$

In case of slender fibers where $r \to \infty$, the terms "$4 \ln 2$" and "-6" in the denominator of the above expression can be neglected. Therefore, the final state of the coefficient A will be as follows:

$$A = \frac{r^2}{4 \ln r}. \tag{3.11}$$

The same approximation can also be done for the coefficient F;

$$F = \frac{3r^2}{\ln(2r) - 0.5} = \frac{3r^2}{\ln 2 + \ln r - 0.5}$$

By considering high aspect ratio fibers again, the first and the third terms in the denominator of the above expression will be neglected. Therefore, the coefficient F reads

$$F = \frac{3r^2}{\ln r}. \tag{3.12}$$

After finding these coefficients, now we can put them in equation ((**3**.**10**) so as to obtain the non-Newtonian stress tensor;

$$\boldsymbol{\tau}^{NN} = \mu \frac{\phi r^2}{\ln r} \boldsymbol{D} : \langle \boldsymbol{nnnn} \rangle + 6\mu \frac{\phi r^2}{\ln r} D_r \langle \boldsymbol{nn} \rangle. \tag{3.13}$$

Equation ((**3**.**13**) can be written in a simpler form as following:

$$\boldsymbol{\tau}^{NN} = \alpha \mu \boldsymbol{D} : \langle \boldsymbol{nnnn} \rangle + 6\alpha \mu D_r \langle \boldsymbol{nn} \rangle, \tag{3.14}$$

in which α is the model parameter and already defined in section 2.4.

With the help of the above findings we now have a simple constitutive equation for the non-Newtonian part of the stress tensor for the Brownian high aspect ratio fibers.

3.2 First Proposal for Brownian Fibers

In this section of this work, we will start explaining our new proposals which are developed to approximate the moments of the orientation distribution function (ODF) in order to reproduce the non-Newtonian stress tensor. The first proposal is given by;

$$\langle \boldsymbol{nn} \rangle = \frac{\boldsymbol{u}'\boldsymbol{u}'}{\boldsymbol{u}' \cdot \boldsymbol{u}'} + \frac{dt}{\tau} 2D_r \left(\langle \boldsymbol{nn} \rangle - \frac{\boldsymbol{I}}{3} \right), \tag{3.15}$$

where

$\langle \boldsymbol{nn} \rangle$ is the second moment of the orientation distribution function in which **n** is a unit vector showing the orientation of the each fiber,

$\boldsymbol{u}'$ is the velocity fluctuation vector

dt is the time step size

τ is the relaxation time constant

D_r is the rotary Brownian diffusivity

$\boldsymbol{I}$ is the identity tensor.

Before testing our first proposal in our flow solver (MGLET), we had to test this model analytically in order to check whether it has some bad behaviors or not. We can simplify equation ((**3**.**15**) as follows:

$$y^{n+1} = b + \tau^{new} dt \left(y^n - \frac{1}{3} \right), \tag{3.16}$$

with initial condition

$$\left(y^0 = \frac{1}{3} \right)$$

where

$$\tau^{new} = \frac{2D_r}{\tau}, \tag{3.17}$$

y^{n+1} is the value at the time step (n+1). It addresses to the second moment of the orientation distribution function. b addresses the velocity fluctuation components, the first term in the right hand side of equation ((**3**.**15**).

In order to check the first proposal, it is modeled with a commercial software. In this work MATLAB is used. Before modeling the above equation, one should notice that τ^{new} will be our driving parameter. We will try to understand the behavior of our model by modifying this parameter. Of course, time step size dt can also be changed. There might be 3 options for defining the "b". You can see these options in figure below. As it is a well known fact that, in turbulent flows, velocity fluctuations act in a random manner. However, for simplicity the below configurations are selected. Since, we only want to see the behavior of our model.

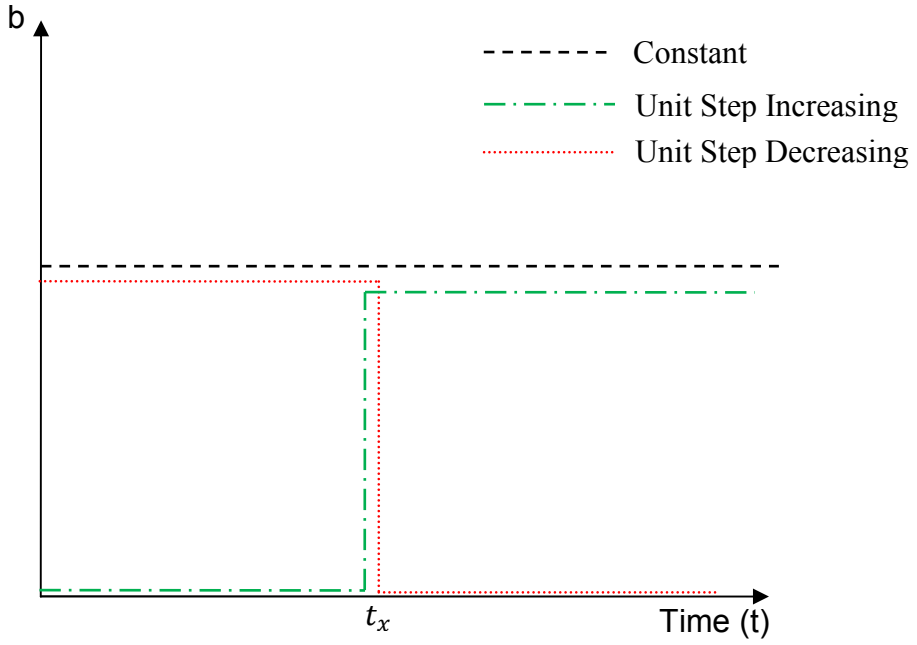

Figure 3.1: Alternative options for the parameter "b"

While modeling the first proposal, we should consider all these options. The results which are showing the behavior of our first proposal have been plotted in figure 3.2. Only the results for the case "unit step increasing" are given. A time step $dt = 0.1$ is selected.

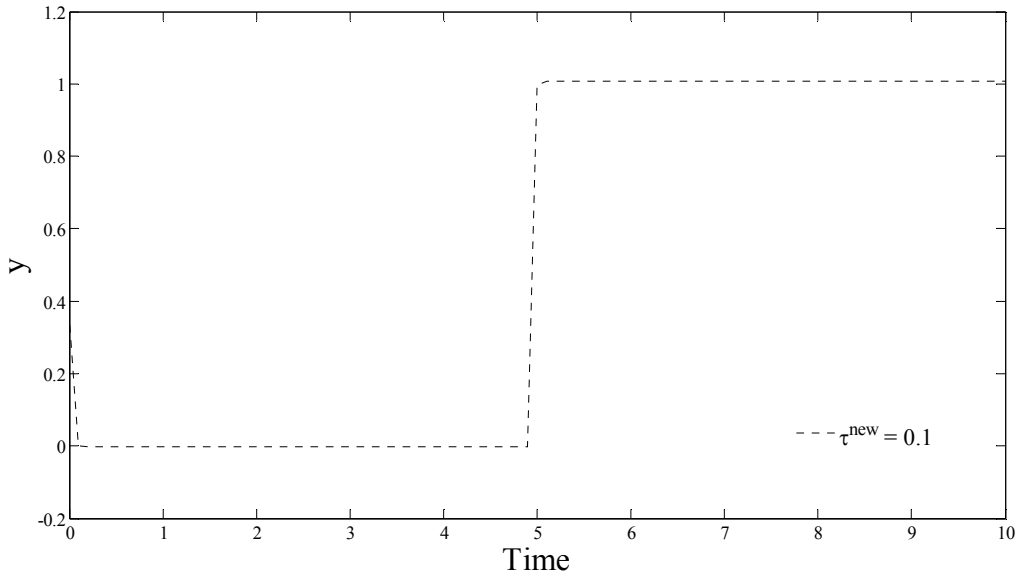

Figure 3.2a: The response of the system for $\tau^{new} = 0.1$

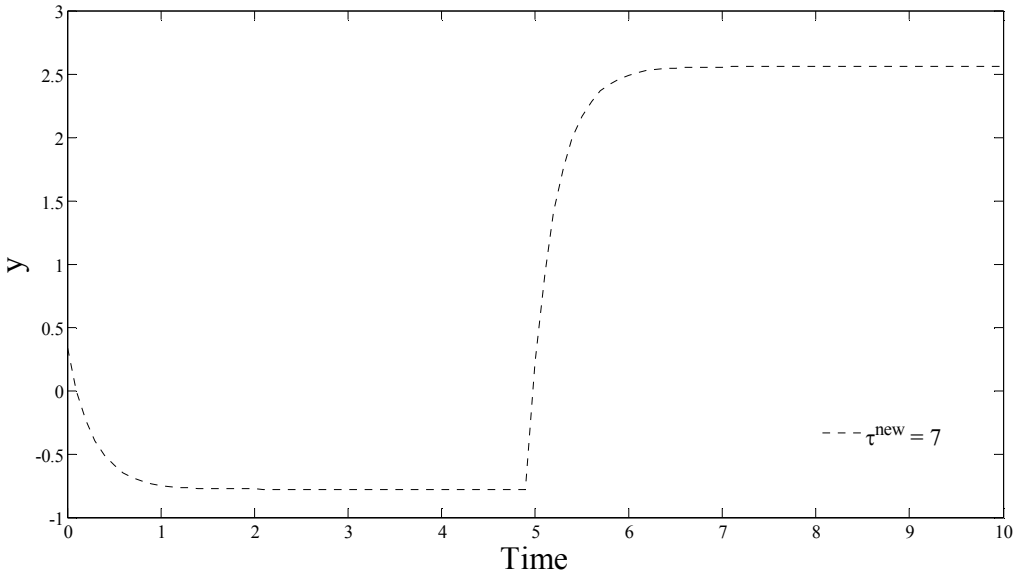

Figure 3.2b: The response of the system for $\tau^{new} = 7$

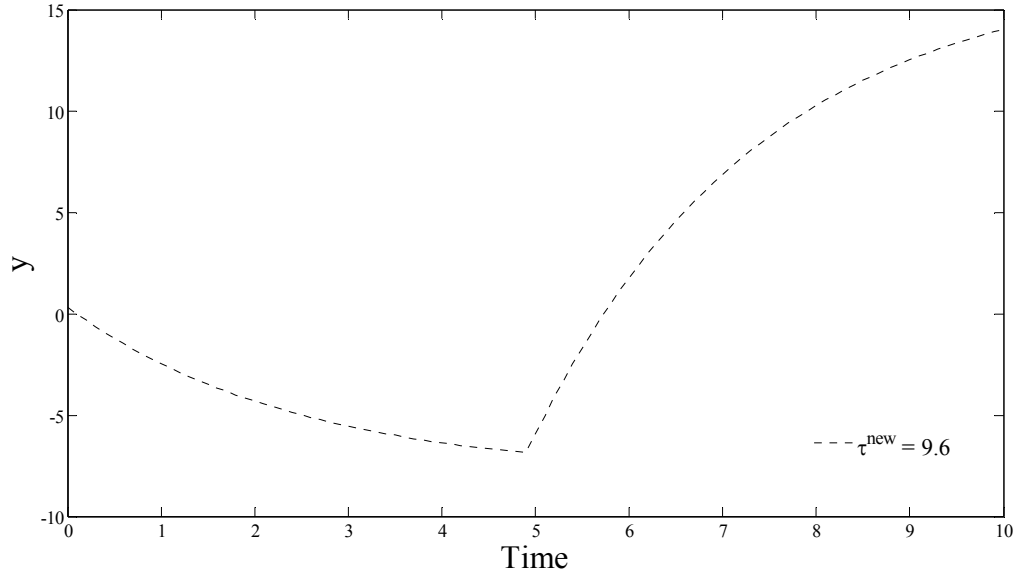

Figure 3.2c: The response of the system for $\tau^{new} = 9.6$

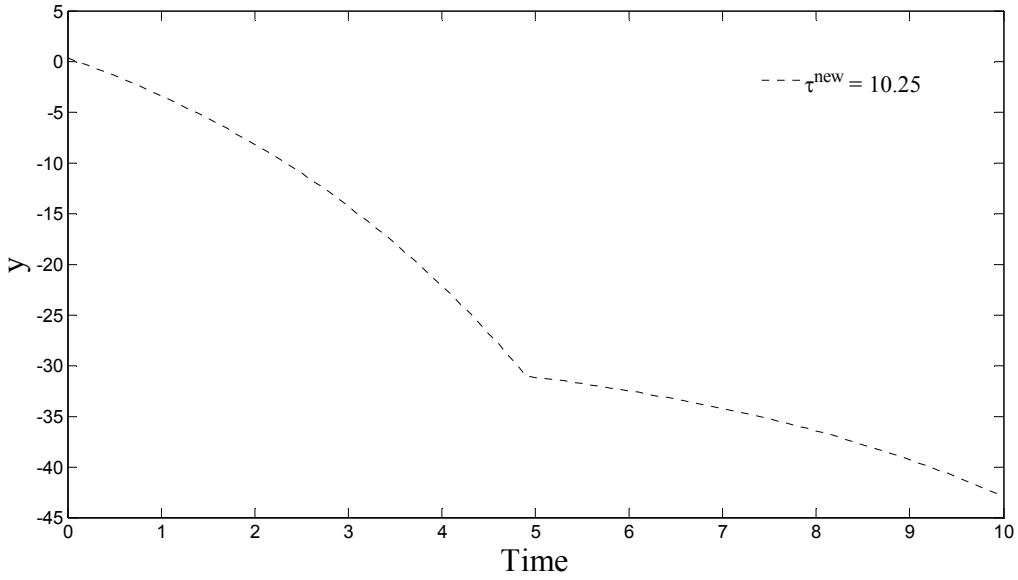

Figure 3.2d: The response of the system for $\tau^{new} = 10.25$

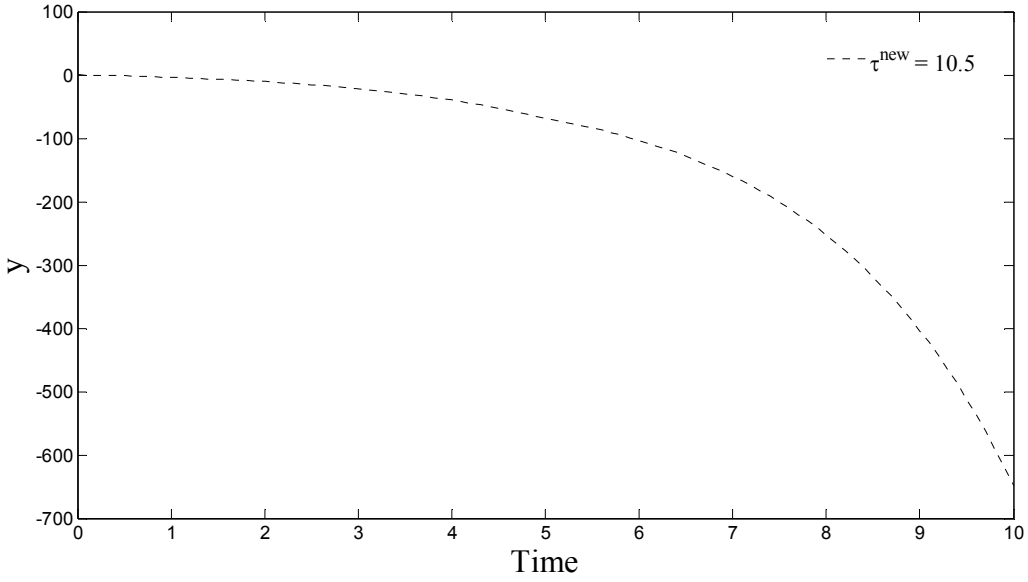

Figure 3.2e: The response of the system for $\tau^{new} = 10.5$

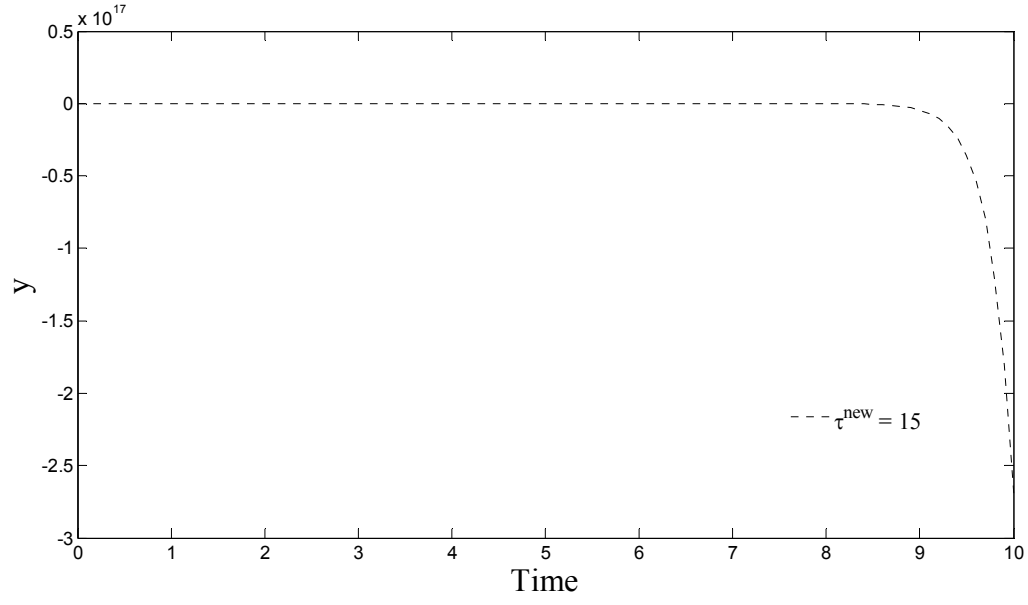

Figure 3.2f: The response of the system for $\tau^{new} = 15$

As we can see in figure 3.2, the response of our system is not stable and the magnitudes are increasing drastically while increasing our driving parameter τ^{new}. Therefore, we need to find an analytical solution for our first proposal to see if it is a well-behaved model or not. Equation ((**3**.**15**) can be written in a more simplified form in order to obtain the analytical solution:

$$y = b + k\left(y - \frac{1}{3}\right), \tag{3.18}$$

where $k = \tau^{new} dt$. If we solve equation ((**3**.**18**) for y, we get

$$y = \frac{3b - k}{3(1 - k)}. \tag{3.19}$$

If we plot this function with $b = 1$, we get the figure 3.3.

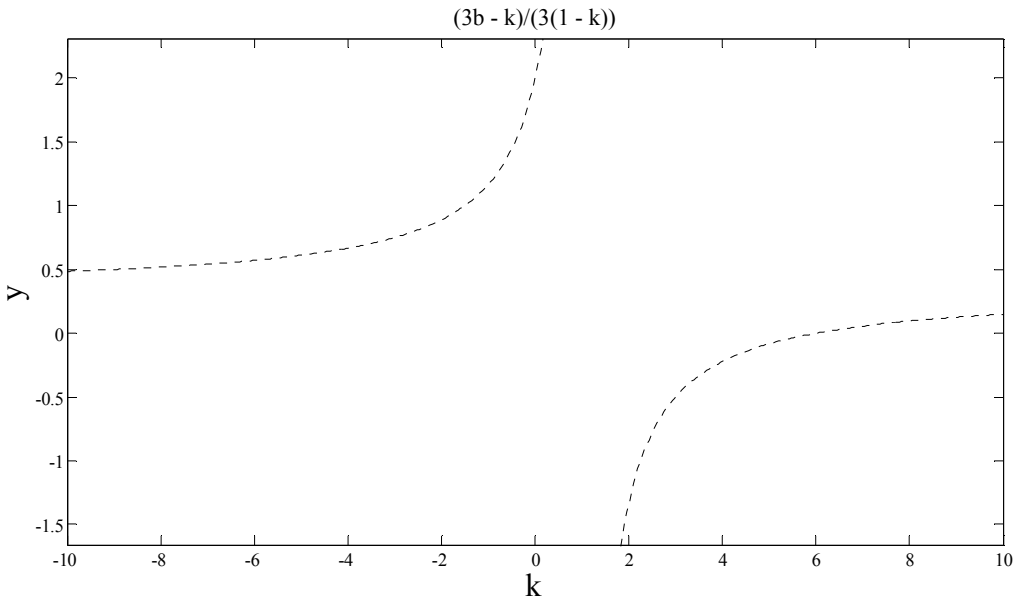

Figure 3.3: Analytical expression of the first proposal

As it can be deduced from the above findings that, we cannot use our first proposal as a new model since it contains some instabilities and magnitudes are reaching infinity which is not desired in fluid dynamics simulations. Therefore, we need to come up with a new idea which does not contain critical points. What we are expecting in our new model is being well-behaved. Thus, we come up with another model which is called viscous anisotropic model with velocity fluctuations with Brownian motion or the VAFB model.

3.3 Second Proposal - VAFB Model

After observing the unstable behavior of the first proposal, we came up with a new proposal for the second moment of the ODF given by

$$\langle \boldsymbol{nn} \rangle = \alpha_{iso} \frac{\boldsymbol{u'u'}}{\boldsymbol{u'} \cdot \boldsymbol{u'}} + (1 - \alpha_{iso}) \frac{\boldsymbol{I}}{3}, \tag{3.20}$$

where α_{iso} is our new driving parameter which is a function of the rotary Brownian diffusivity D_r. α_{iso} can be defined as

$$\alpha_{iso} = e^{-kD_r}, \tag{3.21}$$

where k is a constant which should be determined. It can be understood from equations ((**3**.**20**) and ((**3**.**21**) that, in case of zero Brownian diffusivity $D_r = 0$, the value of α_{iso} will be equal to 1. This case directly produces the VAF model. This is an important property of the second proposal and will be explained in the chapter 5 while presenting the results. Note that, according to equation ((**3**.**21**), in case of strong rotary Brownian diffusivities $D_r \gg 1$, our driving parameter α_{iso} will vanish, so the first term in the right hand-side of equation ((**3**.**20**) will vanish as well. In this situation, the VAFB model will produce the so-called isotropic state. In isotropic state the second moment of the ODF reads

$$\langle \boldsymbol{nn} \rangle = \begin{pmatrix} \frac{1}{3} & 0 & 0 \\ 0 & \frac{1}{3} & 0 \\ 0 & 0 & \frac{1}{3} \end{pmatrix}.$$

In case of isotropic state, we do not see a drag reduction but an increase in total frictional drag. This situation will also be discussed in chapter 5. If we take a closer look at our new proposal, we can see that, it does not contain any critical points which can affect the response of the simulations in a bad way. Therefore, this new proposal can be considered as a well-behaved model. This is an important property that the first proposal fails to satisfy. Now, one can add this new proposal into equation ((**3**.**14**) which is valid for Brownian high aspect ratio ($r > 10$) fibers. Therefore, the non-Newtonian stress tensor for high aspect ratio Brownian fibers can be written as follows:

$$\boldsymbol{\tau}^{NN} = \alpha\mu\boldsymbol{D}:\left(\alpha_{iso}\frac{\boldsymbol{u}'\boldsymbol{u}'}{\boldsymbol{u}'\cdot\boldsymbol{u}'} + (1-\alpha_{iso})\frac{1}{3}\boldsymbol{I}\right)\left(\alpha_{iso}\frac{\boldsymbol{u}'\boldsymbol{u}'}{\boldsymbol{u}'\cdot\boldsymbol{u}'} + (1-\alpha_{iso})\frac{1}{3}\boldsymbol{I}\right) + 6\alpha\mu D_r\left(\alpha_{iso}\frac{\boldsymbol{u}'\boldsymbol{u}'}{\boldsymbol{u}'\cdot\boldsymbol{u}'} + (1-\alpha_{iso})\frac{\boldsymbol{I}}{3}\right). \tag{3.22}$$

The model defined by equation (3.22) is called the VAFB model. The VAFB model also considers the effects of the Brownian motion of the suspended fibers and is an alternative algebraic closure for the non-Newtonian Navier-Stokes equations for dilute Brownian fiber suspensions.

4 SIMULATION SETUP

All simulations have been conducted in a 3D unsteady incompressible flow solver called MGLET which is developed in *"Fachgebiet Hydromechanik"* in *"Technische Universität München"*. The programming language that has been used to develop this code is FORTRAN. MGLET is an efficient flow solver for simulating the turbulent channel flows directly. The flow variables are defined on a non-equidistant Cartesian mesh in a staggered arrangement i.e. pressure is stored in cell centers, and velocity components are stored at the cell faces. Also, the non-Newtonian stress tensor $\boldsymbol{\tau}^{NN}$ is stored at pressure nodes. Refer to Moosaie (2011) for further details. The projection method is used in order to solve the unsteady incompressible Navier-Stokes equations. MGLET uses a second-order accurate, cell-centered finite volume formulation for the spatial discretization, and a low-storage third order Runge-Kutta scheme for the time integration. Poisson equation is solved directly by using the fast Fourier transform in periodic directions (streamwise and spanwise directions) for calculating the pressure at a new time level.

In this master thesis all simulations are conducted in a fully developed turbulent channel flow with a nominal shear Reynolds number $Re_\tau = u_\tau\, h/\nu = 180$. Where h, ν and u_τ are the channel half-width, the kinematic viscosity of the fluid and the shear velocity with the definition; $u_\tau = \sqrt{\tau_w/\rho}$ in which τ_w is the wall shear stress, and ρ is the density of the fluid. The domain, with dimensions $(L_x, L_y, L_z) = (4\pi h, \frac{4}{3}\pi h, 2h)$ is discretized by 180, 140 and 128 grid points in streamwise (x), spanwise (y) and wall-normal (z) directions, respectively. One can see the flow configuration in figure 4.1. The grid is non-equidistant in wall-normal direction, and equidistant in streamwise and spanwise directions. The reason for that is simple i.e. we are dealing with near-wall coherent structures; therefore, need a fine mesh near the wall. Time step size is set to 0.01. All simulations have been conducted in one single CPU.

Periodic boundary conditions are applied in streamwise and spanwise directions, while no-slip boundary condition is assumed in wall-normal direction. Note that our flow solver works with a constant negative mean pressure gradient in streamwise direction. Therefore, one should expect an increase in bulk velocity for the case of drag reduction. There are some groups that are using a constant velocity instead of a constant pressure gradient. In their case, drag reduction is manifested with a decrease in pressure gradient. However, the idea behind both methods is the same, so it is not a problem to work with a velocity driven or a pressure gradient driven model.

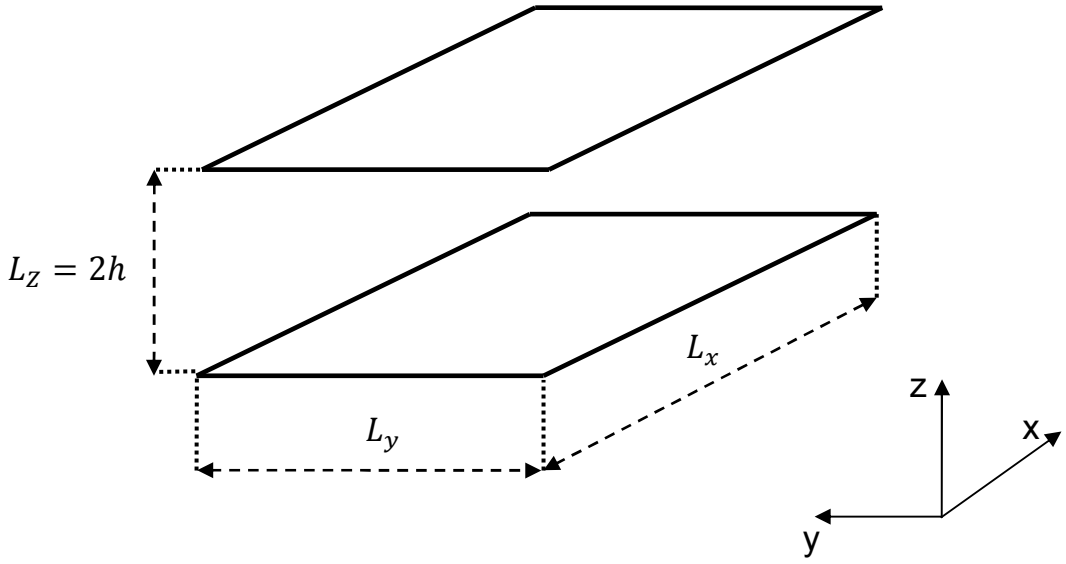

Figure 4.1: Flow configuration showing the dimensions of domain

Note that in this master thesis two-way coupled simulations have been conducted. In two-way coupling there is an interaction happening between the fluid and fiber particles. Due to this interaction, not only the properties of particles are affected by the fluid, but also the fluid properties such as velocity will be affected by the particles. In our two-way coupled simulations a model parameter of $\alpha = 15$ is used. This model parameter is achieved by using an aspect ratio of $r = 100$ and a concentration parameter of $nL^3 = 18$. In order to determine our model constant k, several test cases are considered. This calibration has been done according to the results of Moosaie (2011) in same flow configurations. The determining criterion for this calibration is the bulk velocity. The bisection method is applied in order to find the exact value of k. At Péclet number of $Pe = 1000$, with a constant k=350, the same bulk velocity is reached in both models.

Therefore, the value of k is set to 350. By adding this value in equation ((**3**.**21**), one can obtain our driving parameter α_{iso} as;

$$\alpha_{iso} = e^{-350D_r}. \tag{4.1}$$

After starting the simulations, in order to get statistically reasonable results, first we run the simulations more than 50 flow through time t_{FT} (more than 60000 time steps) in order to let them reach their equilibrium state. Flow through time can be calculated by $t_{FT} = L_x/u_b$. Our main convergence criterion for a simulation is the bulk velocity. When the bulk velocity reaches its equilibrium, first we stop the simulations, then restart them again and let them run at least 25 t_{FT} (more than 30000 time steps) in order to collect better turbulence statistics. In figure 4.2 one can see how the bulk velocity converges its equilibrium value $u_b = 1.112$ for the case $Pe = \infty$.

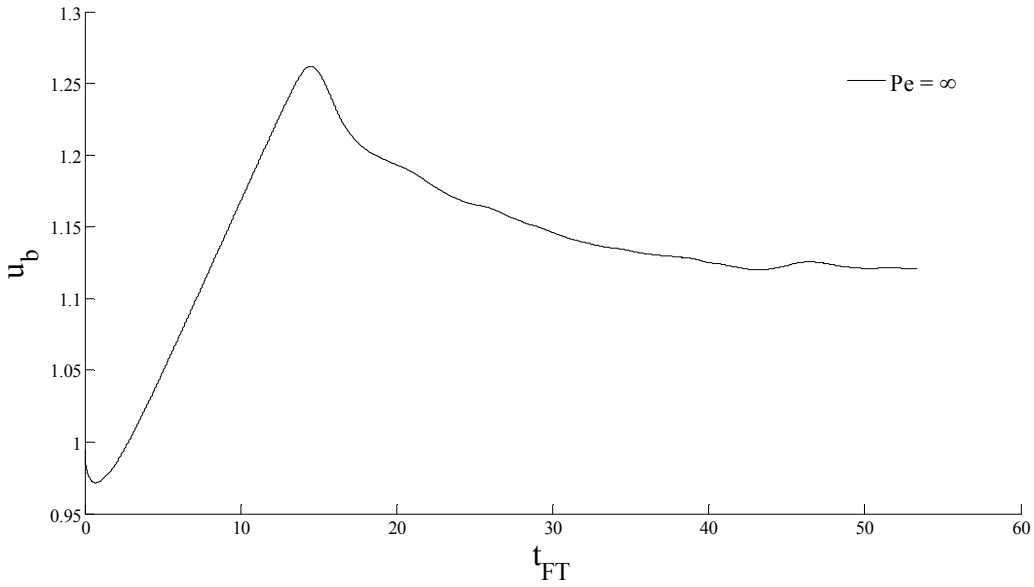

Figure 4.2 : Bulk velocity convergence profile for $Pe = \infty$

5 RESULTS

In this chapter, the results of the two-way coupled simulations of the VAFB model will be presented. However, before presenting the results, I want to make a short summary about the known properties of the turbulent drag reduced flows. In turbulent drag reduced flows, it is found that the streamwise turbulence intensity increases while spanwise and wall-normal turbulence intensities decrease. Also, Reynolds shear stress decreases in case of drag reduction. In addition, of course in a pressure driven flow solver, one should also expect an increase in the bulk velocity, or in the mean streamwise velocity. These are the basic known features of the drag-reduced flows and we will discuss our simulation results by comparing our findings with these known features.

5.1 Mean Streamwise Velocity Profile

In figure 5.1, mean streamwise velocity profile of the Newtonian and the fibrous flows have been plotted with respect to dimensionless wall distance z/h. Note that, for fibrous flows, the VAF model and the VAFB model with $Pe = \infty$ are plotted separately. If we remember the definition of the VAFB model, in case of zero rotary Brownian diffusivity ($D_r = 0$), the second term including the rotary Brownian diffusivity in equation ((**3**.**14**) will vanish. Also, our model constant α_{iso} will be equal to 1 ($\alpha_{iso} = 1$), so the VAFB model will be reduced to the VAF model. Actually, this is a very good property of the VAFB model that we can directly compare the results with those of the VAF model. As it can be understood from figure 5.1, the VAFB model with infinite Péclet number and the VAF model produce the same results. We were expecting this outcome before we run the simulations. As it is explained earlier, the presence of drag reduction is associated with an increase in the bulk velocity or an increase in the mean streamwise velocity. In figure 5.1, one can see that, in the VAFB model, the mean streamwise velocity has been increased considerably when compared to the Newtonian flow. So, it can be said that, the VAFB model is also capable of demonstrating the basic drag reducing behavior of fiber additives.

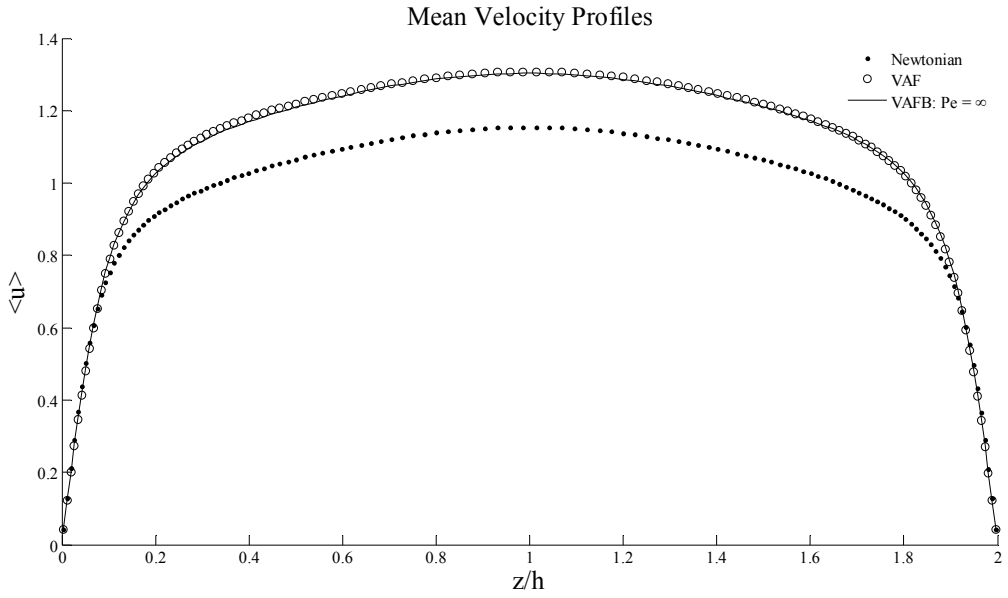

Figure 5.1: Mean streamwise velocity profile of Newtonian and fibrous flows with the VAF and VAFB models with $Pe = \infty$

In figure 5.2 and figure 5.3, the mean streamwise velocity profiles of the fibrous flows with different Péclet numbers are plotted. In these figures, the influence of Péclet number on mean streamwise velocity profiles can be seen clearly. Before running these simulations, we have thought that, by increasing rotary Brownian diffusivity D_r, we should obtain less drag reduction, and also at one specific value of Péclet number the bulk velocity should be equal to the Newtonian state, and by further increase in diffusivity should bring not a drag reduction but a drag increase. Now, if we look carefully to figures 5.2 and 5.3, we can clearly see that our results are in line with theory. First, we get the maximum drag reduction (maximum mean streamwise velocity or max. bulk velocity) in case of infinite Péclet number, in other words maximum drag reduction is observed in case of non-Brownian fibers with zero rotary Brownian diffusivity. This result is in line with the results of Paschkewitz *et al.* [18] who have shown that maximum drag reduction is obtained in case of non-Brownian fibers. As you can see, by increasing rotary Brownian diffusivity, the mean streamwise velocity is decreasing and the mean velocity profiles are getting closer to the Newtonian state. Specifically, with a Péclet number of 100, the mean velocity profiles of the Newtonian flow and this specific Péclet number are nearly the same. This implies that, we can take this Pe as a reference point, and compare with the other results of our simulations.

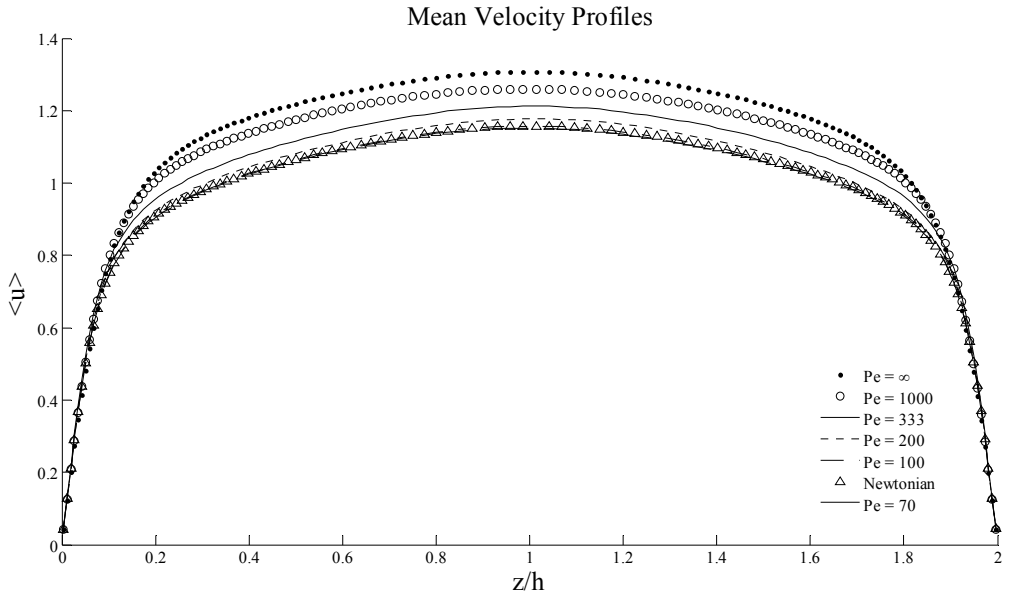

Figure 5.2: Influence of Péclet number on mean streamwise velocity profile

It can be deduced that, with further increase in rotary Brownian diffusivity, we should have a mean velocity profile which is under the Newtonian state in our plot. Therefore, in order to see this effect clearly, the figure 5.3 has been plotted. Figure 5.3 is just a detailed version of figure 5.2. If we look carefully to that figure, we can observe that with a Péclet number of 70, mean streamwise velocity is less than Newtonian case. This means that, although we are using fiber additives in order to decrease the drag in the flow, in case of Brownian fibers which are subjected high rotary Brownian motion; we do not see a drag reduction, but an increase in total drag. These findings are consistent with many theoretical observations in literature for the suspensions of rigid-rod like particles with Brownian motion.

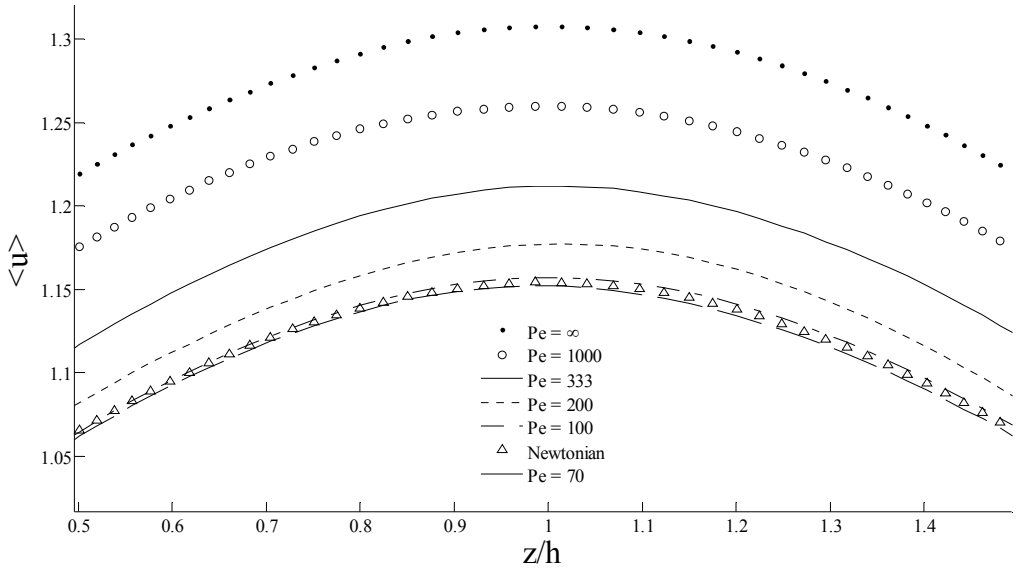

Figure 5.3: A detailed plot for the influence of Péclet number on mean streamwise velocity profile to see the drag increase effect at $Pe = 70$

In figure 5.4 the mean streamwise velocity profiles of the flows with different Péclet numbers have been plotted in wall coordinates. Note that mean streamwise velocities are normalized with shear velocity u_τ. Dimensionless wall distance z^+ is defined by

$$z^+ = \frac{u_\tau z}{\nu}, \tag{5.1}$$

where ν is the kinematic viscosity of the fluid and u_τ is the shear velocity with $u_\tau = \sqrt{\tau_w/\rho}$. The center of channel lies at $z^+ = 180$. The region $z^+ < 5$ is called viscous sublayer. The region $z^+ > 30$ is called logarithmic layer and the region between viscous sublayer and logarithmic layer $5 < z^+ < 30$ is called the buffer layer. We can see in figure 5.4 that all flows with different Pe follows the Newtonian profile throughout the viscous sublayer, and the profiles start to deviate at buffer layer. This situation is reasonable, since the buffer layer, although it is a thin region when compared to the logarithmic region, is the region that contains large scale coherent structures causing a skin friction. Therefore, it is nice to see that the mean streamwise profiles of fiber-induced flows at $Pe = \infty, Pe = 1000, Pe = 333$ and $Pe = 200$ start deviating upward, $Pe = 100$ remains unchanged, and $Pe = 70$ starts deviating downward in buffer layer. Therefore we can clearly understand how the fibers modify these coherent structures that are responsible for the drag production. These deviations cause a shifting in logarithmic

region which is a sign of a change in thickness of the viscous sublayer. For example, for $Pe = \infty, Pe = 1000, Pe = 333$ and $Pe = 200$, the viscous sublayer is thickened, this effect is vice versa for $Pe = 70$. As it is mentioned earlier, this thickening and weakening in the viscous sublayer cause a parallel shifting in mean streamwise velocity profiles in logarithmic layer. In figure 5.4, one can see how the velocity profiles are shifted away from each other. When we compare the velocity profiles of Newtonian flow and fibrous flow with $Pe = \infty$, we can see that the shift is larger than the others which is consistent with a higher drag reduction. As is well known, a drag reduction is manifested as an upward shift in velocity profile, and a drag increase is manifested as a downward shift. In order to see this effect clearly, the figure 5.5 is plotted which is nothing else but a detailed version of figure 5.4. In figure 5.5 one can see the effect of Brownian motion in mean streamwise velocity profiles in wall coordinates. As expected, with a Péclet number of 70, we have observed a downward shift in velocity profile, which is an indication of a drag increase.

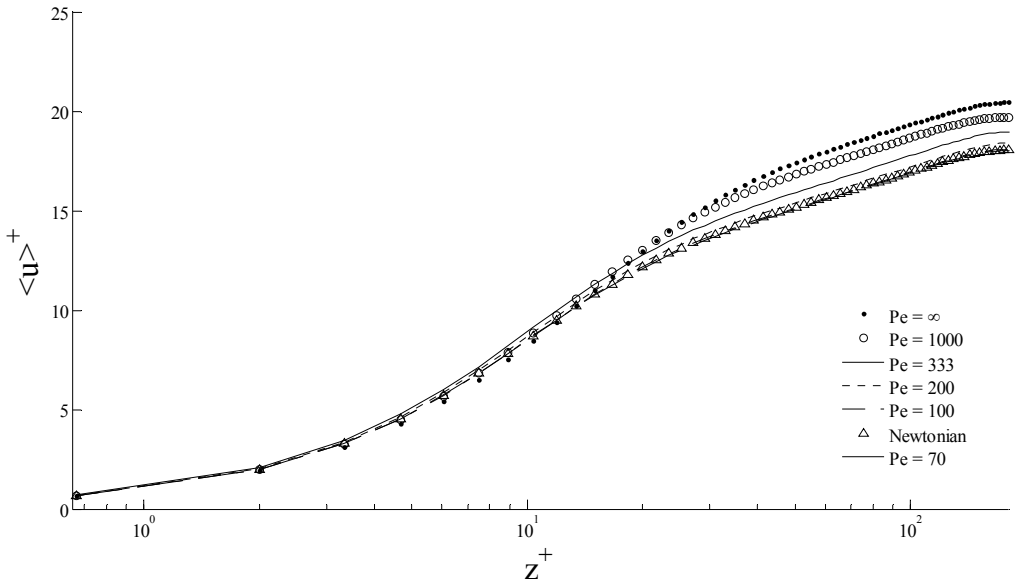

Figure 5.4: Mean velocity profile of the flows with different Péclet numbers in wall coordinates

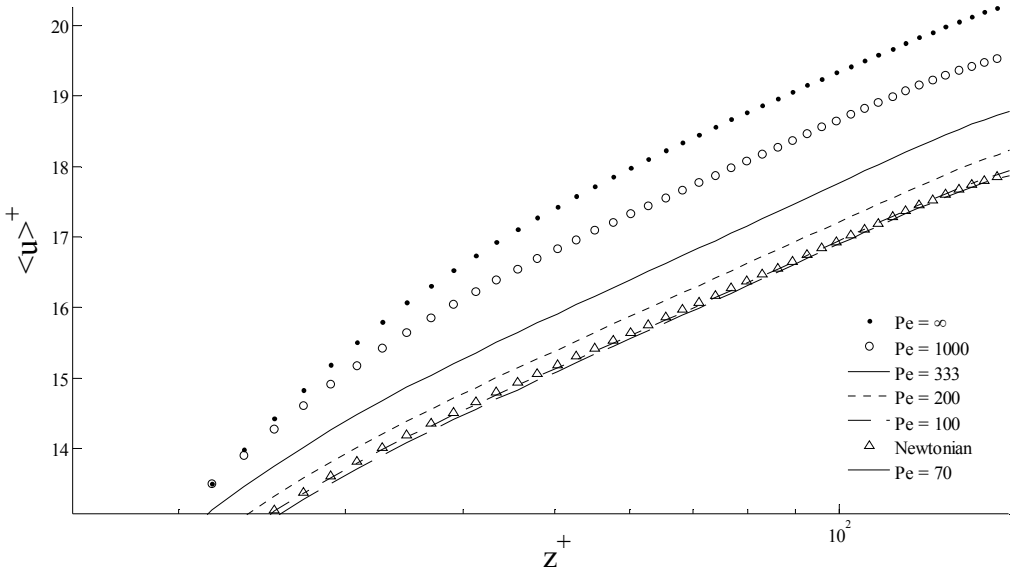

Figure 5.5: A detailed plot for the mean velocity profile of the flows with different Péclet numbers in wall coordinates to see the drag increase effect at $Pe = 70$

The amount of drag reduction can be calculated by $DR = (1 - {u_b}^N/{u_b}^{NN}) \times 100$. Where superscripts N and NN denote the Newtonian, and the non-Newtonian (fibrous) cases, respectively. The bulk velocities of each flow configuration and the amount of corresponding drag reduction are given in table 5.1. The bulk velocity of the Newtonian flow is also shown for reference. As we can see clearly, for $Pe = 70$, we have an increase in frictional drag by 0.57%.

Table 5.1: Comparison of the bulk velocity and drag reduction amounts of different flow cases

Simulation	Bulk Velocity (u_b)	Drag Reduction (%)
Newtonian	0.99	-
$Pe = \infty$	1.11	10.8
$Pe = 1000$	1.09	9.17
$Pe = 333$	1.04	4.80
$Pe = 200$	1.01	1.98
$Pe = 100$	0.99	0
$Pe = 70$	0.986	-0.57

5.2 Turbulence Intensities

Plotting the root-mean-square (rms) profiles of the velocity fluctuations components u', v' and w' versus the wall distance z^+ is an important indicator that shows how the turbulent structure changes by different flow parameters. These rms values are also known as the turbulent intensities. u'_{rms}, v'_{rms} and w'_{rms} are the turbulent intensities in streamwise, spanwise and wall-normal directions, respectively. These intensities are defined as

$$u'_{rms} = \sqrt{\langle u'u' \rangle}, \tag{5.2}$$

$$v'_{rms} = \sqrt{\langle v'v' \rangle}, \tag{5.3}$$

$$w'_{rms} = \sqrt{\langle w'w' \rangle}, \tag{5.4}$$

where $\langle u'u' \rangle$, $\langle v'v' \rangle$ and $\langle w'w' \rangle$ are the diagonal components of the Reynolds stress tensor. The components of the Reynolds stress tensor are defined as following:

$$\tau'_{ij} = -\rho \langle u'_i u'_j \rangle. \tag{5.5}$$

In figure 5.6, turbulent intensity profiles in streamwise direction of different flow types with different Péclet numbers has been plotted. In this figure and the following two figures (figure 5.7 and figure 5.8) turbulent intensities u'_{rms}, v'_{rms} and w'_{rms} are normalized by shear velocity u_τ. Dimensionless turbulent intensities are defined by

$$u'^{+}_{rms} = \frac{u'_{rms}}{u_\tau}, \tag{5.6}$$

$$v'^{+}_{rms} = \frac{v'_{rms}}{u_\tau}, \tag{5.7}$$

$$w'^{+}_{rms} = \frac{w'_{rms}}{u_\tau}. \tag{5.8}$$

We know from the literature that the turbulent intensities are affected by the fibers and they exhibit different features such that while spanwise and wall-normal intensities decrease, streamwise intensity increases considerably in drag-reduced turbulent flows. As

we can see in figure 5.6, streamwise turbulence intensity u'^{+}_{rms} increases with higher Péclet numbers and the peak location shifts outward. This is a sign of thickening in viscous sublayer. We can observe that, in case of infinite Péclet number, the streamwise intensity is maximum, and when the intensity of Brownian motion increases, the streamwise turbulent intensity decreases and at a specific Péclet number, $Pe = 100$, the intensity is nearly equal to that of Newtonian flow.

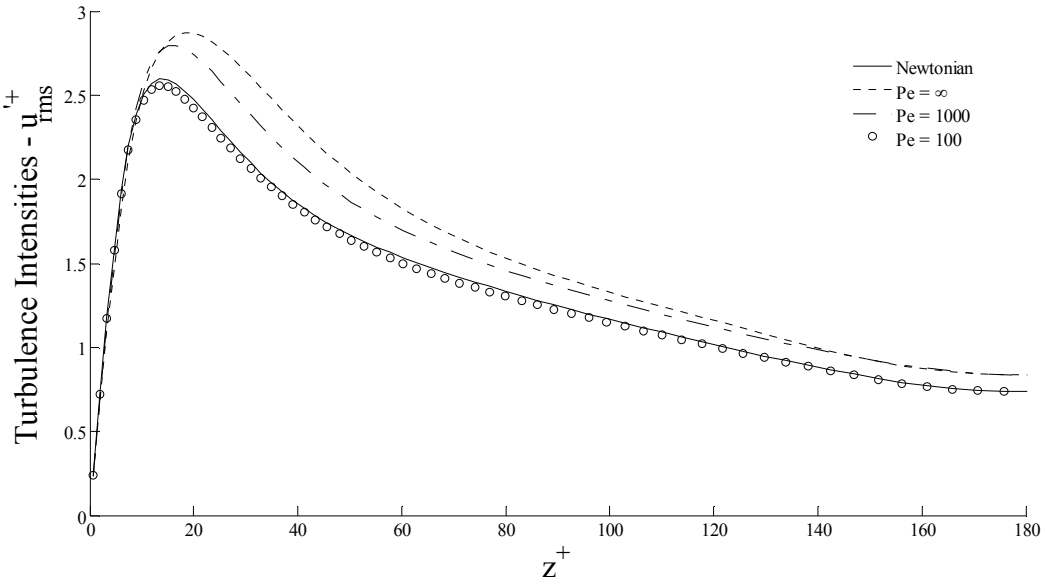

Figure 5.6: Root mean square (rms) of streamwise velocity fluctuations

This result also supports the findings in section 5.1 in which we have found that $Pe = 100$ gives the Newtonian state. Therefore, we are now quite sure that in the VAFB model, this specific value of Péclet number nearly produces the Newtonian state. We can also see in figure 5.6 that when Péclet number increases, the location of the peak is shifted away from the wall which is totally consistent with the findings in the literature for dilute suspensions of Brownian fibers. In figure 5.7 and figure 5.8 the turbulent intensities in spanwise and wall-normal directions are plotted, respectively. As expected, both turbulent intensities are decreased with higher Péclet numbers. This result is consistent with theoretical findings in literature. Again, a perfect agreement has been obseved between the Newtonian flow and fibrous flow with $Pe = 100$. One should also note that, in all of three figures in this section, a very good agreement has been observed for the magnitudes and peak locations of the turbulence intensity profiles with the published papers in literature i.e. den Toonder *et al.* [22], Manhart and Friedrich [13], Moosaie and Manhart

[17] and Moosaie [16]. In summary, the general trend of the Turbulence intensities for the fiber-induced drag-reduced flows has been produced by the VAFB model.

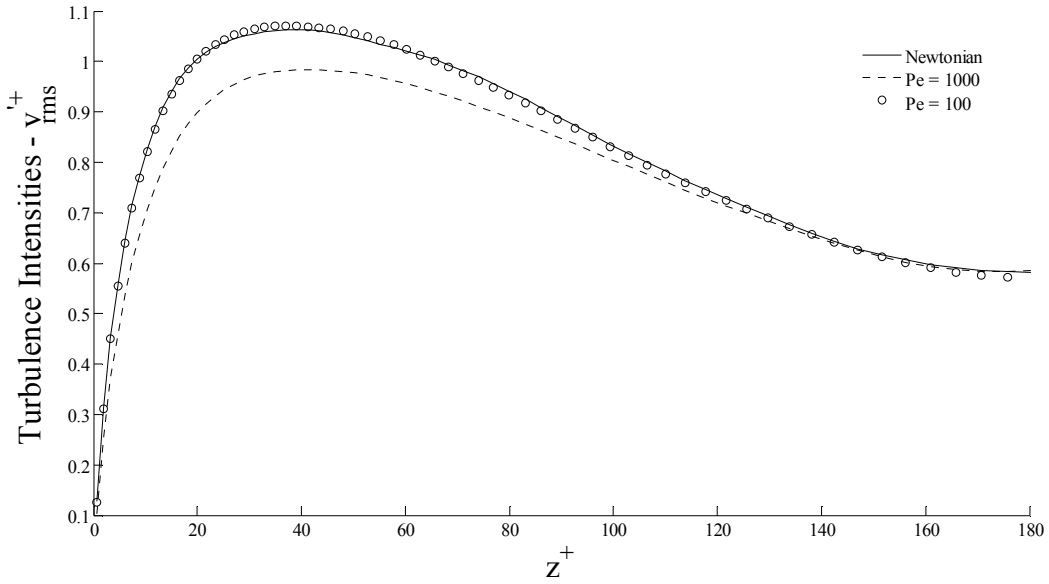

Figure 5.7: RMS of spanwise velocity fluctuations

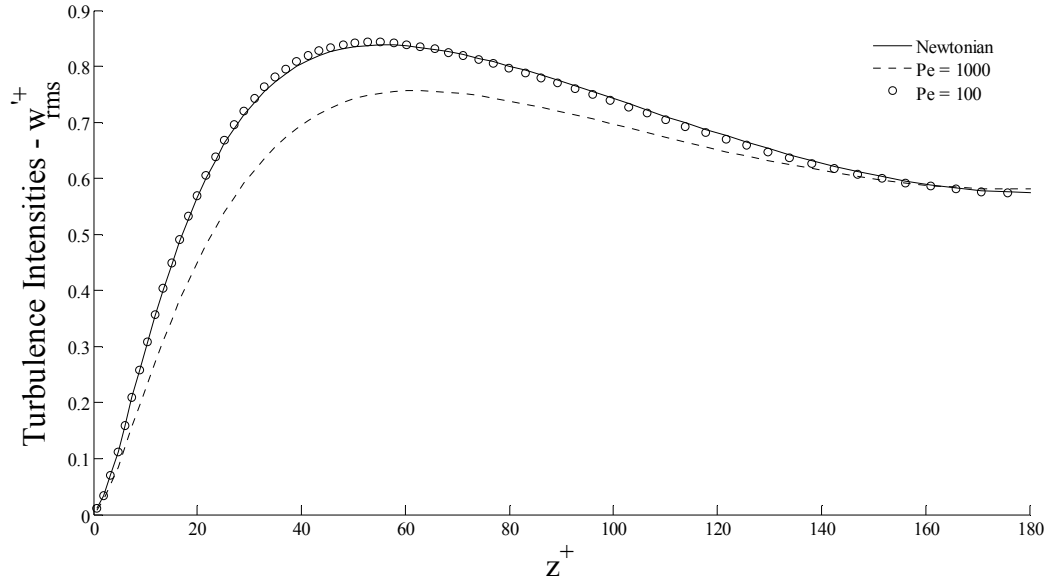

Figure 5.8: RMS of wall-normal velocity fluctuations

5.3 Reynolds Shear Stress

In figures 5.9 and 5.10, the Reynolds shear stress $\langle u'w' \rangle$ profile of the Newtonian flow and the fibrous flows with different Péclet numbers are plotted. As is well known, a drag reduction is always associated with a decrease in Reynolds shear stress compared to the Newtonian flow. It is a widely known fact that, Reynolds shear stress $\langle u'w' \rangle$ is the main source of turbulent kinetic energy production near the wall. Therefore, a decrease in Reynolds shear stresses means that the turbulent structure of the flow is weakening which indicates a drag reduction. Thus, the Reynolds shear stress profiles are very significant indicators for us to see the effects of the Brownian motion in turbulent structure of the flow. In figure 5.9, one can obviously see the effect of the Péclet number in flow. An increase in Péclet number reduces the Reynolds shear stresses. In addition to that, the peak location is shifting away from the wall in case of increasing Péclet numbers. These results are consistent with the findings in literature. Note that, generally, increasing the Péclet number is affecting the flow in the same way that of increasing the term $\alpha\mu$ in equation ((**3**.**14**). Therefore, it is a good property of the VAFB model, that we can compare our results with of several publications in literature.

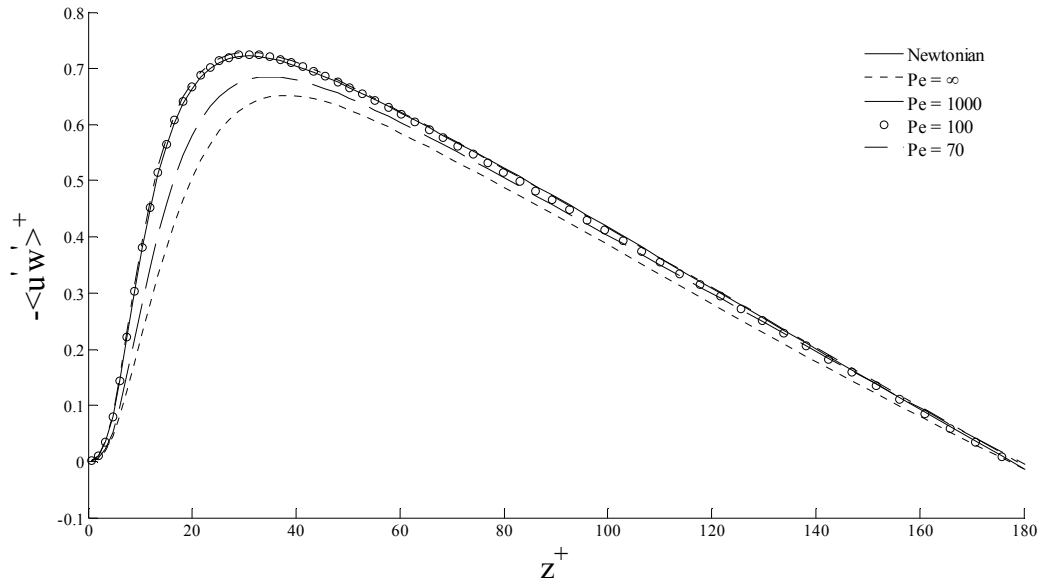

Figure 5.9: Reynolds shear stress $\langle u'w' \rangle$ profile of the Newtonian and fibrous flows with Péclet numbers; $Pe = \infty$, $Pe = 1000$, $Pe = 100$, $Pe = 70$

As it is explained in sections 5.1 and 5.2 , at a specific value of Péclet number the the flow is producing the turbulent statistics of the Newtonian flow. In these sections we have found this value as 100. In case of Reynolds shear stresses this value also holds and at $Pe = 100$, the Reynolds shear stress profiles of Newtonian flow and that specific Péclet number are in a very good agreement. In figure 5.10, there is a detail plot for the Reynolds shear stress profiles. As expected, by further increase in Péclet number from $Pe = 100$ to $Pe = 70$ produces an inverse effect such that Reynolds shear stress is increasing and the peak location is getting closer to the wall. This shows that after this specific value of Péclet number $Pe = 100$, we get not a drag reduction but an increase in frictional drag by further increase in Brownian diffusivity (D_r). This is in accordance with the previous findings in literature and in this master thesis.

5.4 Mean non-Newtonian Stresses

In figure 5.11 and figure 5.12 the mean non-Newtonian stresses $\langle \tau_{11}^{NN} \rangle$, $\langle \tau_{13}^{NN} \rangle$, $\langle \tau_{22}^{NN} \rangle$ and $\langle \tau_{33}^{NN} \rangle$ are plotted in wall coordinates for fibrous flows with two different Péclet numbers, $Pe = \infty$ and $Pe = 1000$, respectively. Note that all stress components have been normalized by $\alpha\mu = \mu\phi r^2 / \ln r$. If we look at these figures we can observe that the normal stress component $\langle \tau_{11}^{NN} \rangle$ exceeds the shear stress component $\langle \tau_{13}^{NN} \rangle$. This observation is consistent with that of Manhart [14] for $r = 100$.

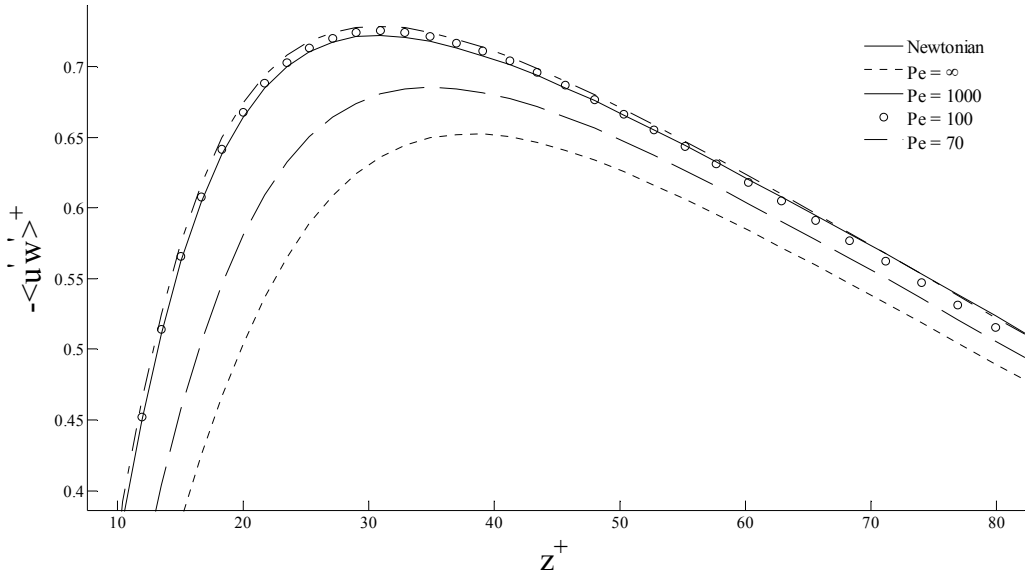

Figure 5.10: A Detailed plot for the Reynolds shear stress $\langle u'w' \rangle$ profile of Newtonian and fibrous flows with Péclet numbers; $Pe = \infty$, $Pe = 1000$, $Pe = 100, Pe = 70$

We can also see that the VAFB model predicts a reasonable normal stress profile i.e. it does not have a negative value away from the wall and has a positive value along the whole layer, and it holds for different values of Péclet number. This is also an important prediction that the VA model cannot provide. In addition, the VAFB model predicts a peak location at a value of $z^+ = 7.5$. The peak location predictions in the VA, VAF and Manhart's full kinetic models are $z^+ = 6$, $z^+ = 8$ and $z^+ = 10$, respectively. This means that the peak location prediction in the VAFB model is also reasonable. Besides, the general non-Newtonian stress profiles of other stress components are in a good agreement with those of full kinetic model. When we increase the intensity of the Brownian motion i.e. decrease the Péclet number we observed that the peak duration is decreasing which is also in accordance with those of full kinetic model. In the VAFB model there is only one thing that we did not be able to match with the findings of full kinetic model. Manhart [14] found that increasing the Brownian diffusivity shifts the peak locations towards the channel and the stresses has a non-zero value at the wall. However, in the VAFB model we did not be able to observe that. Although the last mentioned behavior of the VAFB, it is still capable of showing the fundamental properties of mean non-Newtonian stress profiles.

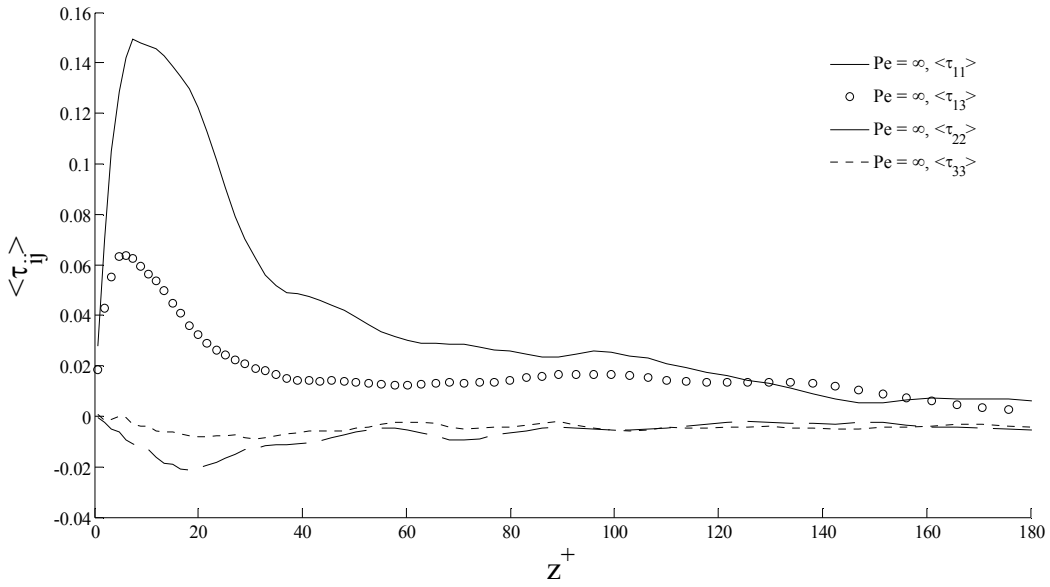

Figure 5.11: Mean non-Newtonian stress profiles for $Pe = \infty$

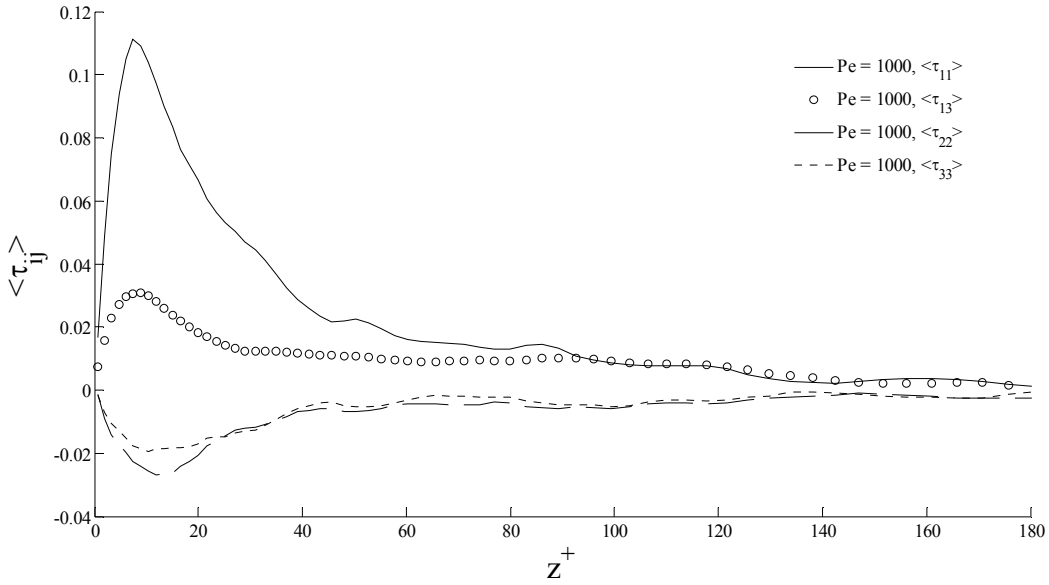

Figure 5.12: Mean non-Newtonian stress profiles for $Pe = 1000$

As a summary, one can understand from the above mentioned results that, the VAFB model exhibits the basic features of the drag-reduced turbulent flows with Brownian fiber suspensions. Generally, the results are in a very good agreement with the previous findings in literature.

6 CONCLUSIONS

In this master thesis, we have presented a brand new model which is capable of showing the general trends of drag reducing behavior of dilute fiber suspensions while taking the Brownian motion of fibers into account. This new model is called the VAFB model. The VAFB model basically is a modification on the VAF model of Moosaie and Manhart [13]. Actually, our new model is an alternative algebraic closure for the non-Newtonian Navier-Stokes equations. Simulations have been conducted by using an existing DNS flow solver called MGLET. The VAFB model provides a significant decrease in computational costs when compared to the direct numerical simulations of the Fokker-Planck equations which have to be solved in order to get the conformation behavior of the fibers.

The VAFB model is tested in a fully developed turbulent channel flow with a nominal shear Reynolds number $Re_\tau = 180$. First, a verification has been done by comparing the findings of the VAFB model with those of the VAF model at the same flow configurations. For this verification, the parameter α_{iso} has been set to 1. A perfect agreement is observed in mean streamwise velocity profiles. Then, several test cases have been implemented with different values of Péclet numbers (Pe) which is a determining parameter for Brownian motion. It has been observed that, mean streamwise velocities are increasing with higher Péclet numbers i.e. maximum mean streamwise velocity has been observed with $Pe = \infty$. These results are in accordance with the findings in literature. It is also noticed that, at $Pe = 100$ the flow statistics of the Newtonian flow is reproduced in the VAFB model. Therefore, it can be said that with further decrease in Pe or a further increase in rotary Brownian diffusivity D_r should result in not a drag reduction but a drag increase. This fact is observed in our results. With a Péclet number of 70, the mean streamwise velocity was lower than that of Newtonian fluid. This is an indicator of the frictional drag increase in a turbulent flow.

In order to obtain more information about the turbulence statistics of the flow, turbulence intensity and Reynolds shear stress profiles have been plotted. With increasing values of Péclet number, the streamwise turbulence intensity is increased while spanwise and wall-normal intensities are decreased. These results are also consistent with previous findings in literature. Also, the peak locations shifted away from the wall with increasing values of Pe which is also in a good agreement with known features in literature. When the intensity of Brownian motion increases, Reynolds shear stress decreases which is also an indicator of drag reduction. By further increasing on rotary Brownian diffusivity (Pe) is resulted in a drag increase as expected.

As a summary, the general drag reducing behavior of the fiber additives with Brownian motion have been reproduced with the VAFB model. The findings in the VAFB model are in a good agreement with previous findings on published data investigating rigid rod-like particle induced wall-bounded turbulent flows.

Bibliography

[1] S. G. Advani and C. L. Tucker. The use of tensors to describe and predict fiber orientation in short fiber composites. *J. Rheol.*, 31:751–784, 1987.

[2] H. Brenner. Rheology of a Dilute Suspension of Axisymmetric Brownian Particles. *Int. J. Multiphase Flow*, 1:195-341, 1974.

[3] W. Brostow. Drag reduction and mechanical degradation in polymer solutions in flow. *Polymer*, 24 :631-638, 1983.

[4] A. Einstein. Über die von der molekularkinetischen Theorie der Wärme geforderte Bewegung von in ruhenden Flüssigkeiten suspendierten Teilchen. *Ann. Physik*, 322:549–560, 1905.

[5] P. G. Gennes. *Introduction to Polymer Dynamics*. Cambridge University Press. 1990.

[6] E. J. Hinch and L. Leal. Constitutive equations in suspension mechanics. Part 1. General formulation. *J. Fluid Mech*., 71:481–495, 1975.

[7] E. J. Hinch and L. Leal. Constitutive equations in suspension mechanics. Part 2. Approximate forms for a suspension of rigid particles affected by Brownian rotations. *J. Fluid Mech*., 76:187–208, 1976.

[8] E. J. Hinch. Mechanical models of dilute polymer solutions in strong flows. *Phys. Fluids,* 20:22-30, 1977.

[9] G. Jeffery. The motion of ellipsoidal particles immersed in a viscous fluid. *Proc. R. Soc.Lond. A*, 102:161–179, 1922.

[10] M. T. Landahl. Drag reduction by polymer addition. In *Theoretical and Applied Mechanics, Proc. 13th Intl. Congr. Theor. and Appl. Mech.* (ed. E. Becker & G. K. Mikhailov), 177-199. Springer, 1973.

[11] W. Lee, R. Vaseleski and A. Metzner. Turbulent drag reduction in polymeric solutions containing suspended fibres. *AIChE J*. 20:128–133, 1974.

[12] J. Lumley. Drag reduction by additives. *Annu. Rev. Fluid Mech*. 1:367–384, 1969.

[13] M. Manhart and R. Friedrich. Direct numerical simulation of turbulent channel flow of a viscous anisotropic fluid, in: H.-J. Bungartz, R. Hoppe, C. Zenger (eds.), Proceedings of the Symposium Organized by the SFB 438 Mathematical Modelling, Simulation and Intelligent Systems on the Occasion of Karl-Heinz Hoffmann's 60th Birthday (Lectures on Applied Mathematics), Munich, 30 June–1 July 1999, *Springer, Heidelberg*, pp. 277–296, 1999.

[14] M. Manhart. Rheology of suspensions of rigid-rod like particles in turbulent channel flow. *J. Non-Newtonian Fluid Mech.*, 112:269–293, 2003.

[15] A. Metzner. Polymer solution and fibre suspension rheology and their relationship to turbulent drag reduction. *Phys. Fluids,* 10:145-149, 1977.

[16] A. Moosaie. Direct Numerical Simulation of Turbulent Drag Reduction by Rigid Fiber Additives, PhD thesis, Technische Universität München, submitted, 2011.

[17] A. Moosaie and M. Manhart. An algebraic closure for the DNS of fiber-induced turbulent drag reduction in a channel flow. *J. Non-Newtonian Fluid Mech.,* 166:11901197, 2011.

[18] J. S. Paschkewitz, Y. Dubief, C. D. Dimitropoulos, E. S. G. Shaqfeh and P. Moin. Numerical simulation of turbulent drag reduction using rigid fibres. *J. Fluid Mech.*, 518:281–317, 2004.

[19] S. B. Pope. *Turbulent Flows*. Cambridge University Press, Cambridge, 2000.

[20] S. Sasaki. Drag reduction effect of rod-like polymer solutions. I. Influences of polymer concentration and rigidity of skeletal back bone. *J. Phys. Soc. Japan*, 60:868–878, 1991.

[21] K. Sreenivasan and C. White. The onset of drag reduction by dilute polymer additives and the maximum drag reduction asymptote. *J. Fluid Mech.* 409:149-164, 2000.

[22] J. M. J. den Toonder, M. A. Hulsen, G. D. C. Kuiken and F. T. M. Nieuwstadt. Drag reduction by polymer additives in a turbulent pipe flow: numerical and laboratory experiments. *J. Fluid Mech.*, 337:193–231, 1997.

[23] P. Virk, H. Mickley and K. Smith. The ultimate asymptote and mean flow structures in tom's phenomenon. *Trans. ASME E: J. Appl. Mech*. 37:488–493, 1970.

[24] Trans Alaska Pipeline System FACTS, *http://www.akresource.org/curriculum_cd/energy/energyresources/alyeska.pdf,* Access 2 December, 2011.